Title	遷移金属窒化物薄膜の電気化学的特性及び電極触媒活性
Author(s)	東, 正志
Citation	大阪大学, 1987, 博士論文
Version Type	VoR
URL	https://hdl.handle.net/11094/2178
rights	
Note	

ELECTROCHEMICAL AND ELECTROCATALYTIC PROPERTIES OF TRANSITION-METAL NITRIDE THIN FILMS

by

Masashi AZUMA

LABORATORY FOR CHEMICAL CONVERSION OF SOLAR ENERGY
AND DEPARTMENT OF CHEMISTRY
FACULTY OF ENGINEERING SCIENCE
OSAKA UNIVERSITY

1987

ELECTROCHEMICAL AND ELECTROCATALYTIC PROPERTIES OF TRANSITION-METAL NITRIDE THIN FILMS

by

Masashi AZUMA

LABORATORY FOR CHEMICAL CONVERSION OF SOLAR ENERGY
AND DEPARTMENT OF CHEMISTRY
FACULTY OF ENGINEERING SCIENCE
OSAKA UNIVERSITY

1987

Contents

Preface

Various electrochemical cells, such as Zinc-Chlorine, or Sodium-Sulfur secondary batteries, redox-flow cells, fuel cells, water electrolysis cells, and photoelectrochemical cells, have recently been attracting strong attention from the view point of conversion and storage of electric as well as solar energy. In the studies of these cells, the common important problem is to find efficient and stable electrode materials. Noble metals such as platinum and iridium in general have high electrochemical stability and catalytic activity, and are used as electrode materials in phosphoric acid-type fuel cells, for instance. However, these materials are very expensive and it is keenly desired to find other low-cost, stable and active electrode materials. Carbon is chemically stable, but it has only low electrocatalytic activity for most important energy-converting reactions such as oxygen evolution, oxygen reduction, hydrogen evolution, etc. Carbon has a problem also in that it swells when gas evolution reactions occur on its surface due to the intercalation of evolved gases.

Transition-metal nitrides such as TiN, ZrN, HfN and TaN have attracted much attention in these days as new materials for mechanical use, because they have high melting points (2900 to 3400°C) and hardness (micro-hardness 1000 to 1600 kg/mm^2) [1] compared with the respective transition-metals (mp. 1670 to 3000°C, and hardness 14 to 18 kg/mm^2). These properties suggest that chemical bonds in the transition-metal nitrides are very strong. Transition-metal nitrides are also interesting in that they have metallic conductivity (13 to 22 x 10^{-6} Ω cm) [2], and are fairly easily prepared in the form of thin layers by various methods such as chemical vapor deposition, reactive sputtering technique, and thermal nitridation.

For the purpose of investigating the possibility of employing transition-metal nitrides as efficient and stable electrode materials, we have prepared various nitride films on carbon substrates by the reactive RF sputtering technique and studied their electrochemical properties. Electrochemical studies have so far been made on transition-metal nitrides such as TiN [3-6], VN [5], NbN [7] and TaN [7]. These studies have only shown that the transition-metal nitrides behave like the respective metals, namely, they are either passivated (TiN [5], NbN [7] and TaN [7]) or dissolved (VN [5]) into aqueous solutions in anodic potentials. Quite contrary to these reported results, we have found that niobium nitride (NbN_x) and zirconium nitride (ZrN_x) films are very stable in aqueous solutions in a wide pH region and can cause oxygen and chlorine evolution. These properties are in sharp contrast to Nb and Zr metals. These nitrides also showed high electrocatalytic activity for the oxygen evolution in alkaline solutions. These interesting properties of NbN_x and ZrN_x were obtained because we prepared these nitrides on electrochemically stable carbon substrates. In the previous studies mentioned above, the nitrides were prepared in the form of polycrystalline films by thermal nitridation of metal plates under a nitrogen (or ammonia) atmosphere, and little attention was paid to the penetration of electrolyte solutions through grain boundaries or cracks of the nitride films, which may cause passivation of the underlying metal substrates.

In the first chapter, we will describe the chemical composition and the surface structure of the deposited ZrN_x and NbN_x films and their electrocatalytic activity for the oxygen and chlorine evolution. It is shown that these nitride film electrodes are covered only with very thin surface oxide layers (a few nanometers or less) and have the electrocatalytic activity for the oxygen evolution comparable to or even a little higher than that of smooth nickel electrodes that are known to be the best practical electrode for alkaline electrolysis. The reaction mechanism for the efficient oxygen evolution is discussed on the basis of the surface chemical stucture revealed by XPS studies.

In the second chapter, we will compare the electrochemical stability of the ZrN_x and NbN_x films with that of titanium nitride (TiN_x) and vanadium nitride (VN_x). The NbN_x and ZrN_x films are quite stable and evolve oxygen under anodic potentials as mentioned above, whereas the VN_x films are dissolved into electrolyte solutions and the TiN_x films are rapidly passivated in a way similar to the respective metals. These results cannot be explained by discussions based on the thermodynamic decomposition potentials. A tentative explanation is given by taking account of matching between the distance of M-N bonds in the nitride films and that of M-O bonds in the oxide overlayers.

In the third chapter, we will describe oxygen reduction reaction to form water on cobalt nitride (Co_xN) film electrodes. It is shown that, though a Co metal electrode causes only two-electron-transfer type oxygen reduction to hydrogen peroxide, the Co_xN electrodes cause four-electron-transfer type reduction reaction to water with the electrocatalytic activity similar to platinum electrode that is known to be the most efficient electrode for the oxygen reduction. The oxygen-reduction mechanism is discussed on the basis of that in the reported fairly efficient oxygen reduction on $Co-N_4$ chelate compounds such as Co-phthalocyanines and Co-porphyrins.

In conclusion, we have made electrochemical and surface-analytical studies of some transition-metal nitrides (TiN_x, NbN_x, ZrN_x, VN_x and CoN_x) and revealed, for the first time, that some of these nitrides show electrochemical properties superior to the respective metals. These results indicate that the nitridation of transition metals is an effective way for finding new, low-cost and active electrode materials.

References

1. L. E. Toth, "Transition Metal Carbides and Nitrides", Academic Press, New York (1971).
2. New Ceramics Konwakai (Ed.), "New Ceramics", Nikkan Kogyo Shinbun-sha, (1977).
3. I. I. Vasilenko, N. N. Nechiporenko and D. M. Bubai, Chem. Abst., 75 (1971) 115240u.
4. N. Tamari and A. Kato, Denki Kagaku (English), 44 (1976) 477.
5. Y. Matsuda, M. Inoue, M. Morita, Y. Takasu, H. Mizuno and H. Miura, Denki Kagaku (English), 50 (1982) 258.
6. M. Morita, Y. Yonehara, Y. Matsuda, H. Mizuno and H. Miura, Denki Kagaku (English), 50 (1982) 755.
7. M. Morita, F. Tachihara, Y. Matsuda and H. Mizuno, Denki Kagaku (English), 53 (1985) 504.

Chapter 1.

Oxygen and Chlorine Evolution on Niobium- and Zirconium-Nitride Amorphous Thin Film Electrodes Prepared by the Reactive RF Sputtering Technique.

Summary

Niobium nitride (NbN_x) and zirconium nitride (ZrN_x) amorphous thin film electrodes, deposited on carbon substrates by the reactive RF sputtering technique, are electrochemically stable in aqueous solutions of pH 0 to 14, and cause oxygen or chlorine evolution under anodic polarization, although Nb and Zr metal electrodes are easily oxidized and passivated under such anodic conditions. XPS studies show that these nitride electrodes are covered with very thin oxide layers (about a few nm thick) even after prolonged flow of oxygen evolution current. The electrocatalytic activity of the NbN_x and ZrN_x electrodes for the oxygen evolution increased with the hydroxide ion concentration in solution, and was in strong alkaline solutions comparable to or even a little higher than that of a smooth nickel electrode known to be the best practical electrode for the oxygen evolution. The mechanism of the oxygen evolution reaction on these nitride electrodes is discussed.

Introduction

Transition-metal nitrides have recently been attracting much attention because they have excellent properties such as high melting points, mechanical hardness, metallic electrical conductivity, etc. Electrochemical properties of these materials in aqueous solutions have been studied for titanium nitride [1-4], vanadium nitride [3], niobium nitride [5], and tantalum nitride [5]. It has been shown that these materials are either passivated (TiN [3], NbN [5] and TaN [5]) or dissolved (VN [3]) in aqueous solutions under anodic polarization, like the respective metals.

We have been studying the electrochemical properties of various transition-metal nitride films prepared by the reactive RF sputtering technique. Contrary to the reported results mentioned above, we found that amorphous thin films of niobium nitride (NbN_x) and zirconium nitride (ZrN_x) were electrochemically stable in aqueous solutions in a wide pH region, and cause oxygen or chlorine evolution under anodic potentials [6-8]. The reason why such interesting properties of the NbN_x and ZrN_x were found in our work is probably that we deposited the nitride films on electrochemically stable carbon substrates which did not degrade even if the electrolyte solution penetrate onto the carbon substrates through cracks or pin-holes of the nitride films. In the studies reported by other workers [1-5], the metal nitrides were prepared in the form of poly-crystalline films by the method of chemical vapor deposition on metal substrates or thermal nitridation of metal plates, and little attention has been paid to the reaction of the underlying metal substrates caused by the penetration of electrolyte solutions through the grain boundaries or cracks of the films.

The NbN_x and ZrN_x film electrodes are interesting not only because they are electrochemically stable, but also because they are electrocatalytically active for the oxygen evolution in alkaline solutions. As is well recognized, the oxygen evolution reaction should play an important role in the conversion and storage of electric or light energy [9]. Ruthenium dioxide and other ruthenium-containing metal oxides were reported to be highly active for the oxygen evolution [10] but expensive. Nickel electrodes are known as a low-cost and efficient anode for the electrolysis of water in alkaline media, but they have a problem in that they gradually lose the activity with time due to the formation of high-resistance surface oxide [11]. Our previous finding that the ZrN_x and NbN_x electrodes have the oxygen-evolution activity as high as or even slightly higher than that of smooth Ni electrodes [6-8] is thus significant for deriving new, low-cost and active electrode materials for the oxygen evolution.

It should also be worthwhile to note that the nitride films studied in this work contain only IV- and V-A group elements, while all reported active electrode materials for the oxygen evolution, to our knowledge, contain one or more VIII-A group elements such as Ru, Rh and Ni. Studies on these nitrides might therefore give a new insight into the understanding of the oxygen evolution reaction.

In this chapter we will report results of detailed studies on the surface chemical structure of the NbN_x and ZrN_x film electrodes and their electrocatalytic activity for the oxygen evolution reaction, together with discussions on the oxygen evolution mechanism.

Experimental

Zirconium and niobium nitride (ZrN_x and NbN_x) films were prepared by the reactive RF sputtering technique using an ULVAC SBR-1104E apparatus. Carbon plates (Kyowa Carbon Industry, 2 mm thick), used as substrates, were cut into pieces 10 mm x 10 mm, polished with emery paper and with 0.5 μm alumina powder, rinsed, immersed into dilute aqua regia for several seconds in order to remove metallic impurities, rinsed, degreased by immersing in boiling acetone, and then dried at room temperature. The carbon substrates thus cleaned were set in the sputtering apparatus and cleaned further by sputter-etching using nitrogen plasma for more than 30 min, and then the zirconium or niobium nitride was sputter-deposited under discharge in (3.0 to 8.0) x 10^{-3} Torr (1 Torr = 133.3 Pa) high-purity nitrogen (Neriki Gas, 99.9995%), using a respective metal plate as a target. The Zr and Nb metal plates (99.9% purity) were obtained from The Japan Lamp Industry. The RF power applied was 2.5 W cm^{-2}, and the deposition rate was 4.0 ± 0.4 nm min^{-1} for the ZrN_x films and 5.0 ± 0.5 nm min^{-1} for the NbN_x, as calculated from the weights of the deposited films and the specific gravities of the ZrN_x and NbN_x films assumed to be 7.32 and 5.43 g cm^{-3}, respectively. In all the experiments, the sputter-deposition was carried out for about 3.0 h, yielding the average thickness of the deposited films of 0.70 ± 0.07 μm for ZrN_x and 0.90 ± 0.10 μm for NbN_x.

The deposited films were inspected with an Akashi Seisakusho

ALPHA 30A scanning electron microscope, and the crystal structure was investigated with a Shimadzu VD-1 X-ray diffractometer. The chemical composition was analyzed with a Shimadzu ESCA 750 apparatus. The binding energies for the XPS peaks were in most cases corrected by taking the C 1s peak of contaminating carbon at 285.00 eV as the standard. The relative atomic concentrations were calculated from integrated peak intensities corrected for the relative ionization cross sections.

The ZrN_x and NbN_x electrodes were prepared by soldering a copper wire with silver paste on the rear face of the carbon substrate and by sealing with epoxy resin so that only the nitride face was exposed to electrolyte solutions. Electrochemical measurements were made at room temperature using a Pyrex cell equipped with a ZrN_x- or NbN_x-film (working) electrode, a Pt counterelectrode, and a saturated calomel electrode (SCE) as the reference electrode. Electrolyte solutions were prepared by use of analytical-grade chemicals, and water purified with a Milli-Q Water Purification System of Japan Millipore Corp. The cell solutions were deaerated by bubbling with nitrogen. Current-potential curves were measured with a potentio-galvanostat (Hokuto Denko, HA-101), a function generater (Hokuto Denko, HB-107B) and an X-Y recorder. Tafel characteristics were obtained under a quasi-steady-state galvanostatic condition, by first keeping the current density at 100 mA cm^{-2} for 10 min and then lowering it stepwise and keeping it for 2 min at each step.

Results

1. Characterization of Sputter-Deposited Zirconium- and Niobium-Nitride Films. Figure 1 shows a scanning electron micrograph of a ZrN_x film, sputter-deposited on a carbon substrate in an average thickness of ca. 0.70 μm. The micrograph preserves the granular structure of the carbon substrate, and we could not detect any particle structure on the ZrN_x film formed on carbon substrate even at higher magnification (x 50000). Since the ZrN_x film deposited on slide glass by the same method shows a uniform layer, we can conclude that the deposited ZrN_x film covers the carbon substrate fairly uniformly. For the case of NbN_x, the nitride takes the form of fine grains of 0.1 μm in size and is deposited rather evenly on the surface of carbon particles about 1 μm in diameter [6].

Figure 2 shows X-ray diffraction (XRD) patterns for NbN_x and ZrN_x films deposited on slide-glass plates. The XRD patterns for the NbN_x and ZrN_x films deposited on carbon substrates were essentially the same as those in Fig. 2 except that they were complicated by peaks from the crystalline carbon substrates. The NbN_x film showed no diffraction peak in a range of the diffraction angle (2θ) from 30° to 110°, though hexagonal NbN crystals prepared by the thermal nitridation of Nb metal are reported [12] to show clear peaks, at points marked in Fig. 2(a) by vertical lines with Miller indices in parentheses and relative peak heights in brackets. The ZrN_x films also showed no XRD peak

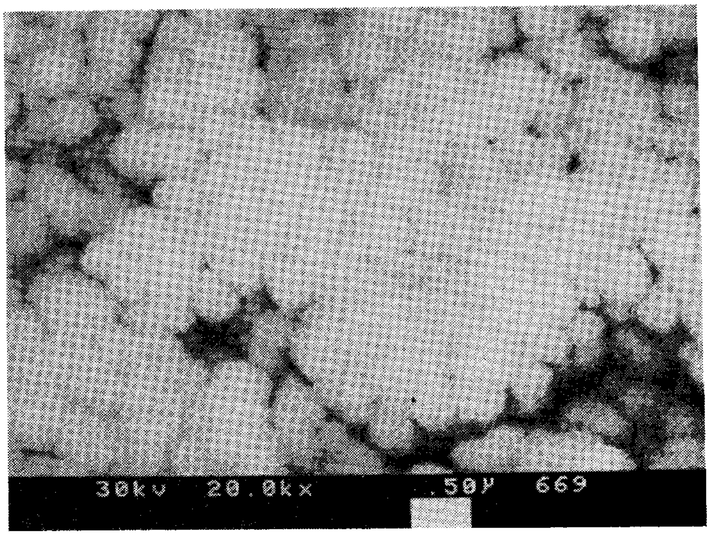

Fig. 1 Scanning electron micrograph of a ZrN_x film deposited on a carbon substrate.

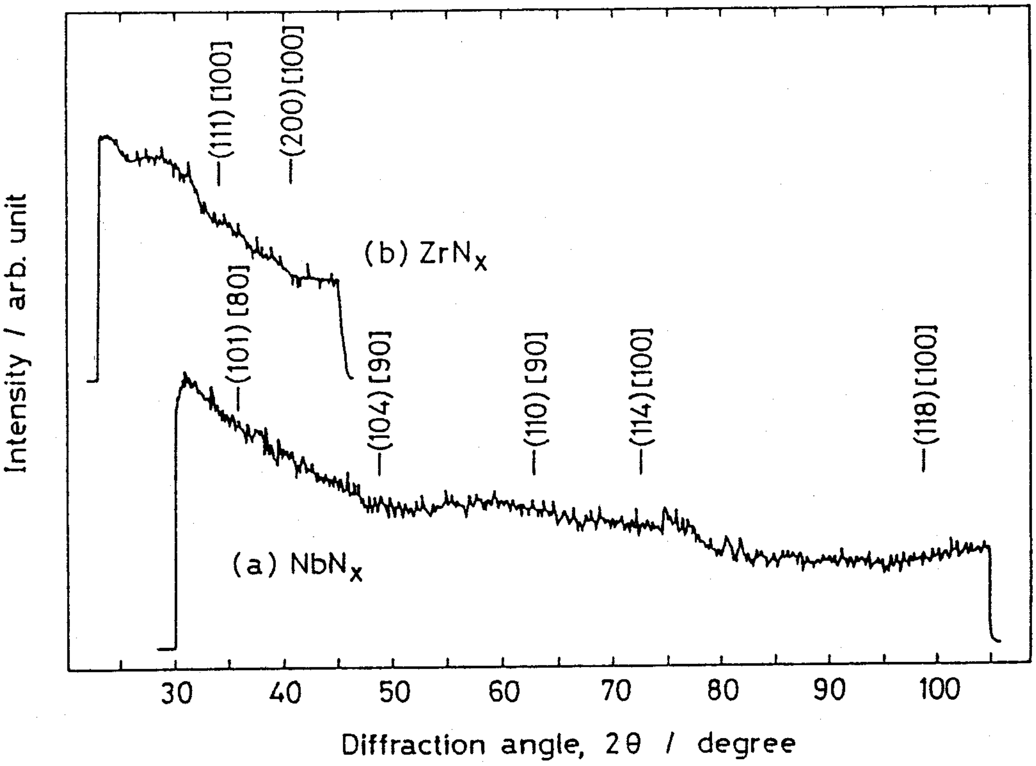

Fig. 2 X-ray diffraction (XRD) spectra for NbN$_x$ (0.90 μm thick) and ZrN$_x$ (0.70 μm thick) films deposited on slide glass substrates. Vertical lines indicate XRD-peak positions reported for the hexagonal NbN crystal and the cubic ZrN crystal. Numerals in parentheses show Miller indices, and those in brackets show relative peak heights.

in a range of 2θ from 25° to 45° (Fig. 2 (b)), though cubic ZrN crystals should show two strong peaks at 34.0° and 39.4° [13]. These results indicate that the NbN_x and the ZrN_x films in the present work are amorphous or, at least, in the form of micro-crystals of a few nm or less in size. The XRD spectra were not changed by thermal treatment at 500°C for 2.0 h under nitrogen atmosphere.

Figure 3 shows XPS spectra for Nb 3d (left) and N 1s (right) peaks for the NbN_x film deposited on a smooth Si substrate. Spectrum (a) was measured for an as-deposited film with no Ar^+-ion etching, whereas spectrum (b) was measured after the Ar^+-ion etching for 1.0 min. This spectrum (b) was unchanged by further etching, indicating that there was no surface impurities. The two Nb 3d peaks at 204.5 eV and 207.2 eV can be assigned to the Nb $3d_{5/2}$ and $3d_{3/2}$ peaks, respectively. In spectrum (a), the peak at around 207.2 eV is stronger than in spectrum (b), and a peak appeared at 210.0 eV. Since niobium oxide prepared by thermal oxidation of an Nb metal plate in air shows Nb 3d peaks at 207.5 and 210.0 eV with nearly the same intensities, spectrum (a) can be explained by the oxidation of the surface of the deposited NbN_x film. The thickness of the surface oxide layer was roughly estimated to be about 2 to 3 nm by assuming that the etching rate for this oxide is the same as that for SiO_2, 10 nm/min. The N 1s peak in spectrum (a) was at an energy somewhat lower than that in spectrum (b) observed after the 1-min

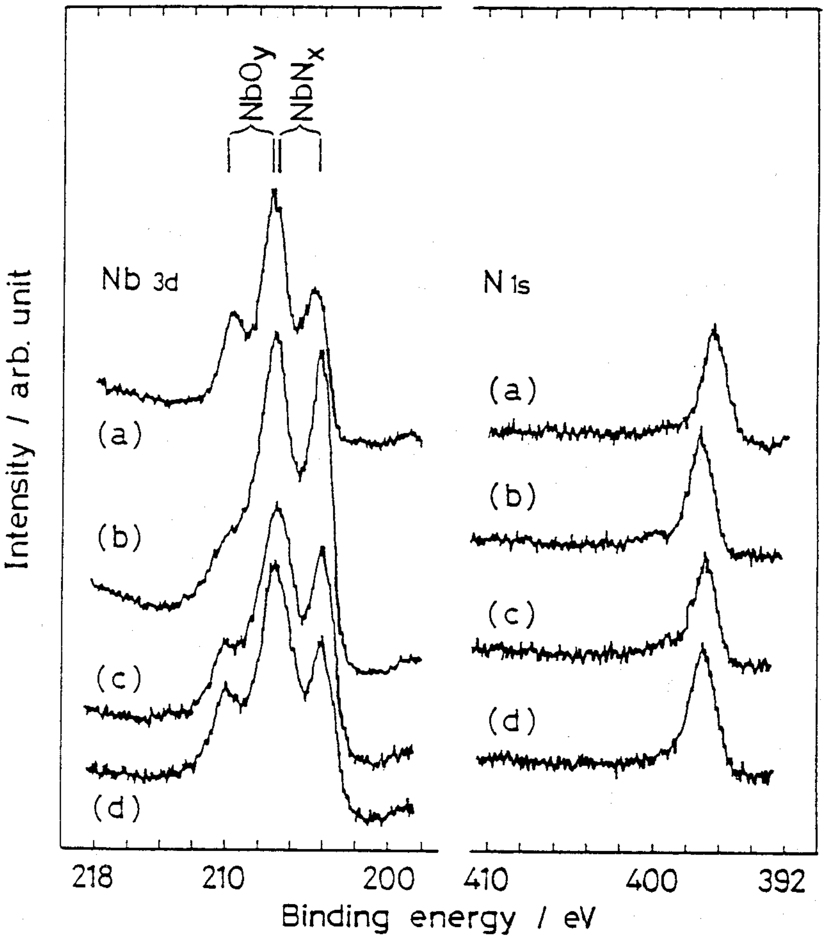

Fig. 3 XPS spectra for Nb 3d and N 1s peaks; (a) for an NbN_x film deposited on a smooth Si wafer with no Ar^+-ion etching, (b) for the same film after the 1-min Ar^+-ion etching, (c) for the NbN_x film deposited on a carbon substrate just after chemical etching in 5% HF, and (d) for the same film after the passage of oxygen evolution current of 10 mA cm^{-2} for 200 s in 0.5 M H_2SO_4. No Ar^+-ion etching was done for (c) and (d).

sputter etching.

Figure 4 shows relative atomic concentrations (A.C.) for the NbN_x film as a function of the Ar^+-ion etching time, together with the binding energies for the N 1s and the Nb $3d_{5/2}$ peaks. The (N/Nb) atomic ratio was about 1.2 at the surface, but it gradually decreased with the Ar^+-ion etching time, finally attaining a constant value of 0.90 ± 0.10 in a region of the etching time longer than 2 min. This ratio is not corrected for the (unknown) difference in the sputter-etching rates between Nb and N. In the present study, the niobium nitride films of the above chemical composition is designated as NbN_x afterwards. The binding energy for the Nb $3d_{5/2}$ peak in the NbN_x film was 1.3 eV higher than that for the corresponding peak in the Nb metal, but about 3.0 eV lower than that for the Nb oxide (NbO_y).

The oxygen concentration in the depth profile in Fig. 4 (lower part) includes a contribution from contaminating oxygen in the XPS apparatus. Accordingly, the amount of oxygen present in the NbN_x film was estimated from the intensities of the Nb $3d_{5/2}$ and $3d_{3/2}$ peaks assigned to niobium oxide relative to those assigned to NbN_x in the XPS spectra (cf. Fig. 3), by assuming that the peaks assigned to the niobium oxide arose from niobium atoms having at least one oxygen atom in the nearest coordination sphere. The atomic ratio of such Nb atoms to the whole ones thus calculated was ca. 23% at the surface (i.e., for no Ar^+-ion etching) and almost zero in the bulk (for the etching time longer

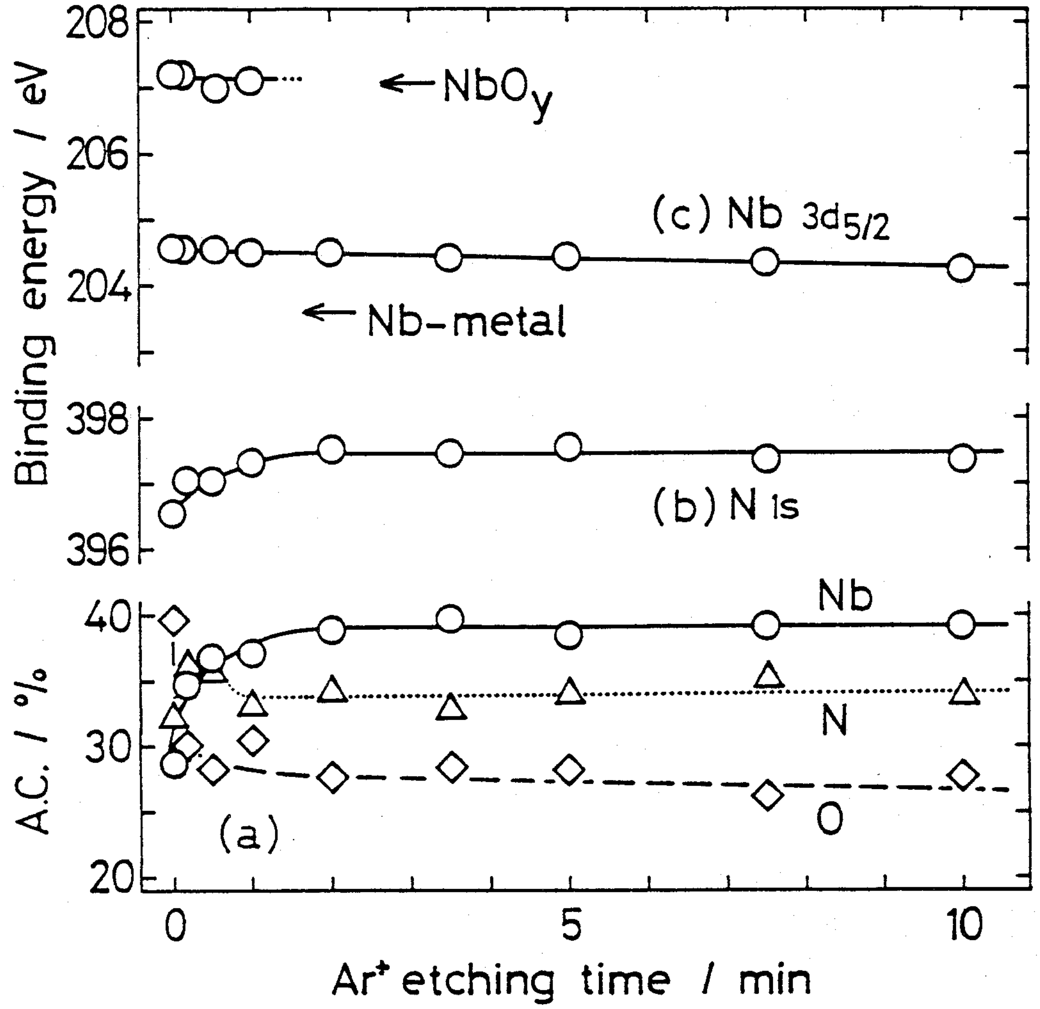

Fig. 4 Relative atomic concentrations (A.C.) for an NbN_x film the same as shown in Fig. 3 (a) and (b) as a function of the Ar^+-ion etching time, together with the binding energies for the N 1s and the Nb $3d_{5/2}$ peaks with the C 1s peak taken as the energy standard.

than 2 min). It is to be noted that the actual (O/Nb) atomic ratio at the surface is expected to be much smaller than that value since one oxygen atom should cause the shifts in the Nb 3d peaks of several Nb atoms surrounding it.

Figure 5 shows XPS spectra for Zr 3d and N 1s peaks for a ZrN_x film deposited on an Si substrate. In a manner similar to Fig. 3, spectrum (a) for no Ar^+-ion etching showed two sharp Zr $3d_{5/2}$ and $3d_{3/2}$ peaks at 180.90 and 183.00 eV, and a weak shoulder at a higher energy, c.a. 185 eV. Since zirconium oxide prepared by thermal oxidation of Zr metal shows the Zr $3d_{3/2}$ peak at 185.20 eV, this shoulder indicates that the surface of the ZrN_x film was slightly oxidized. The shoulder became quite weak by the 10-s Ar^+-ion etching, as shown in spectrum (b). This spectrum was unchanged by further etching, indicating that it was for the ZrN_x film. The thickness of the oxide layer was roughly estimated to be about 1 nm or less by assuming that the etching rate for this oxide is the same as that for SiO_2, 10 nm min^{-1}.

Figure 6 shows relative atomic concentrations for the ZrN_x film, together with the binding energies for the N 1s and the Zr $3d_{3/2}$ peaks. The (N/Zr) atomic ratio was 1.10 ± 0.10 at the surface and 0.95 ± 0.07 in a region of the etching time longer than 10 s. This (N/Zr) ratio is not corrected for the difference in the sputter rate between Zr and N. The films of such a composition are designated hereafter as ZrN_x. The binding energies for the Zr 3d peaks were shifted slightly to lower

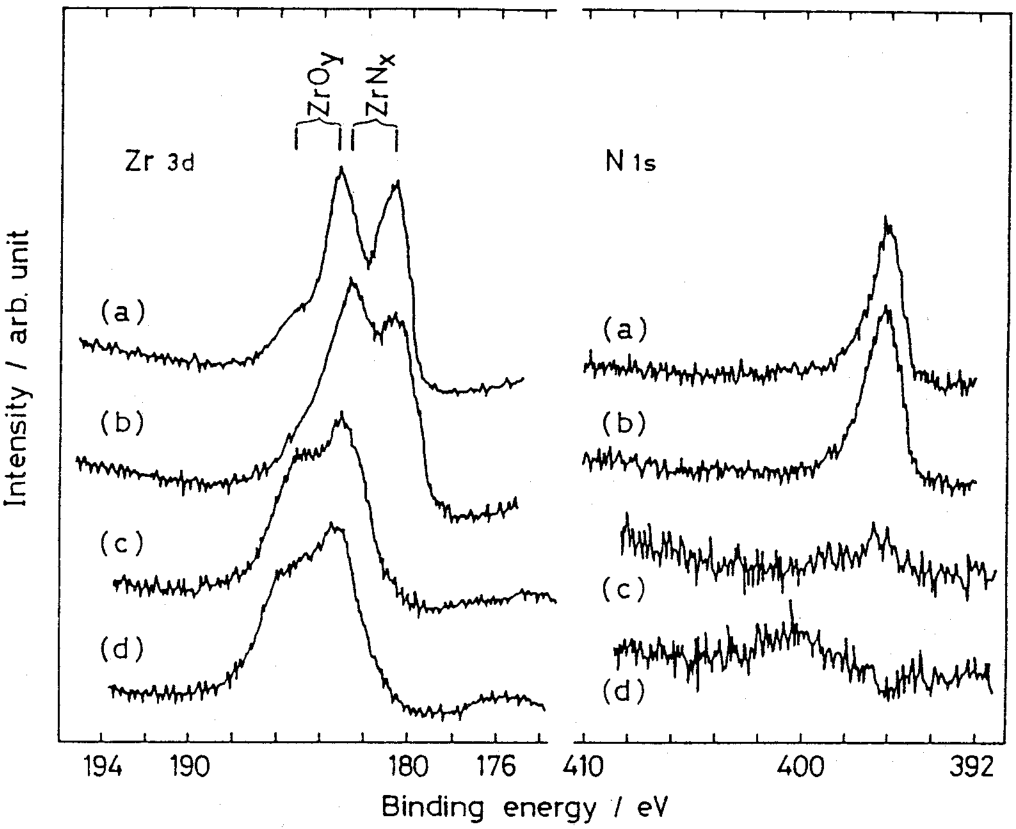

Fig. 5 XPS spectra for Zr 3d and N 1s peaks; (a) for a ZrN_x film deposited on a smooth Si wafer with no Ar^+-ion etching, (b) for the same film after the 10-s Ar^+-ion etching, (c) for the ZrN_x film deposited on a carbon substrate just after chemical etching in 5% HF, and (d) for the same film after 2.4 mC (20 mA cm^{-2}, 120 s) passage of oxygen evolution current in 0.5 M H_2SO_4.

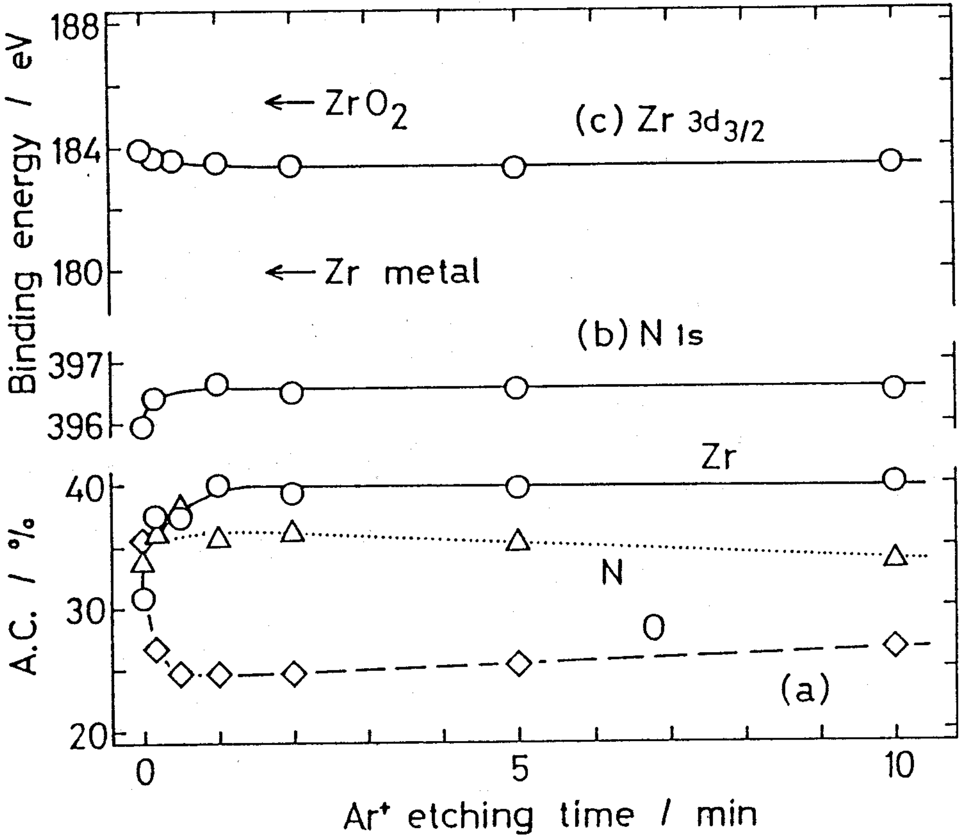

Fig. 6 Relative atomic concentrations (A.C.) for a ZrN_x film the same as shown in Fig. 5 (a) and (b) as a function of the Ar^+-ion etching time, together with binding energies for the N 1s and the Zr $3d_{3/2}$ peaks with the Au $4f_{7/2}$ peak taken as the energy standard.

energies and the N 1s peak shifted slightly to a higher energy by the 10-s Ar^+-ion etching (cf. Fig. 5 (a) and (b)). The binding energy of the Zr $3d_{5/2}$ peak for the ZrN_x film was 1.4 eV higher than that for zirconium metal but 2.2 eV lower than that for ZrO_2.

The electrical resistivities of both the NbN_x and the ZrN_x films were 10^{-4} to 10^{-2} Ω cm, as measured for specimens deposited on slide-glass by taking electrical contacts with silver paste.

2. Electrochemical Properties. Curve a in Fig. 7 shows a typical cyclic voltammogram for an NbN_x film electrode in a 0.5 M H_2SO_4 (M = mol dm^{-3}) solution, and curve b is for an Nb metal electrode. Curve c is for a carbon-plate electrode which is of the same material as those used as the substrate for the NbN_x deposition. The NbN_x electrode was etched in 5% HF for several seconds before the measurement. The niobium metal electrode was easily passivated in the first forward (negative to positive) scan, whereas the NbN_x electrode showed stable voltammograms at repeated scans for more than 1 h. The anodic current for the NbN_x electrode steeply rose at ca. 1.6 V vs. SCE, accompanied by vigorous gas evolution at the surface, indicating that this anodic current corresponds to oxygen evolution. Since the carbon substrate underlying the NbN_x film exhibits the oxygen evolution current only above 2.0 V (curve c), the anodic current arising at 1.6 V is concluded to be due to the oxygen evolution on the NbN_x surface, not on the carbon substrate. Similar results were obtained in neutral and alkaline solutions, except that the onset potential for the anodic current shifted toward the negative with the solution pH [6].

The Nb 3d and N 1s XPS spectra for the NbN_x film electrode etched in 5% HF, and those measured after the passage of the oxygen evolution current of 10 mA cm^{-2} for 200 s in 0.5 M H_2SO_4 are shown in Fig. 3 (c) and (d), respectively. These spectra were nearly the same as that for the NbN_x film just deposited (a),

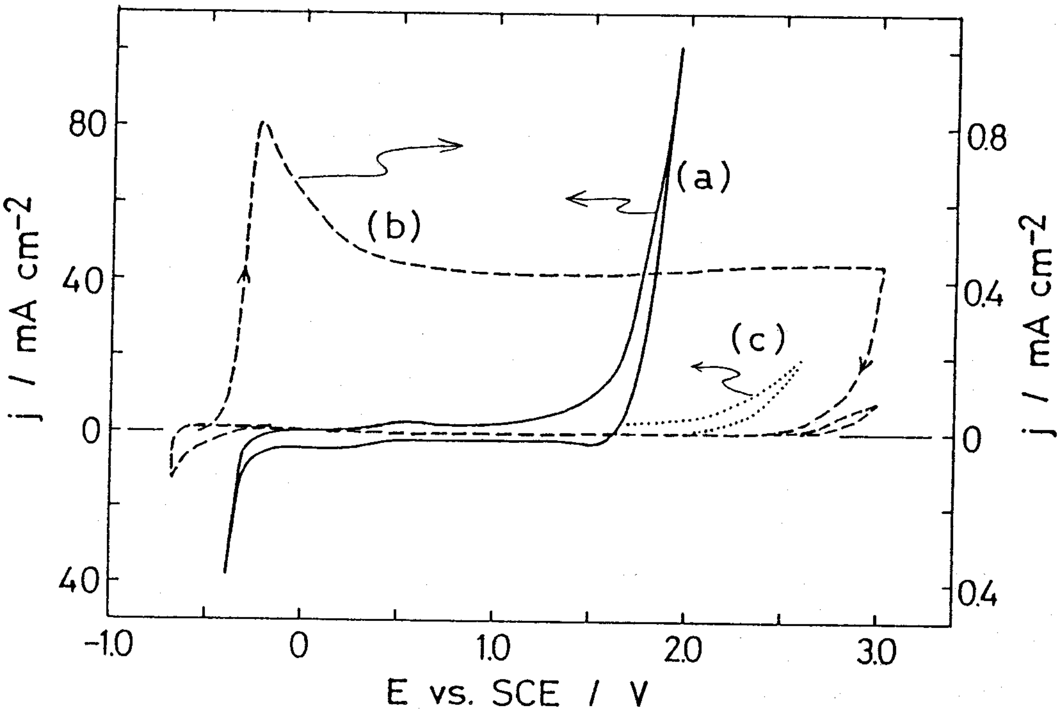

Fig. 7 Cyclic voltammograms for NbN_x (a), Nb metal (b), and a carbon plate used as the substrate for the NbN_x deposition (c), in 0.5 M H_2SO_4 at room temperature. Note that the current density scales are different between curves (a) and (b). The scan rate is 50 mV/s.

namely, no growth of the niobium oxide and nitrogen oxide was observed by the passage of the oxygen evolution current.

Curve a in Fig. 8 shows a cyclic voltammogram for a ZrN_x film electrode in 1.0 M KOH, curve b for a Zr metal electrode and curve c for a carbon-plate electrode. Similar to the NbN_x electrode, the ZrN_x electrode showed a stable oxygen evolution current during repeated cyclic scans for more than 1 h, though the Zr electrode was rapidly passivated in the first forward scan. Similar volammograms were obtained in 0.5 M H_2SO_4 [7] and 0.5 M Na_2SO_4 (pH 4.3).

The Zr 3d and N 1s XPS spectra for the ZrN_x electrode etched in 5% HF for several seconds are shown in Fig. 5 (c). Contrary to the case of NbN_x (Fig. 3), the specrta were quite different from those for the as-deposited ZrN_x film (Fig. 5 (a)) and rather similar to those for zirconium oxide, indicating that the HF-etched ZrN_x film was covered with a zirconium oxide layer. The spectra measured after the passage of the oxygen evolution current of 20 mA cm^{-2} for 120 s in 0.5 M H_2SO_4 (Fig. 5 (d)) were nearly the same as those for the HF-etched electrode. Figure 9 shows a depth profile for the ZrN_x electrode on which the oxygen evolution current was passed. The surface oxide layer was removed by about 1-min Ar^+-ion sputter etching, indicating that its thickness is about 5 nm. The HF-etched ZrN_x electrode and the electrode that was simply immersed in 0.5 M H_2SO_4 for 120 s gave similar depth profiles, suggesting that the ZrN_x surface was

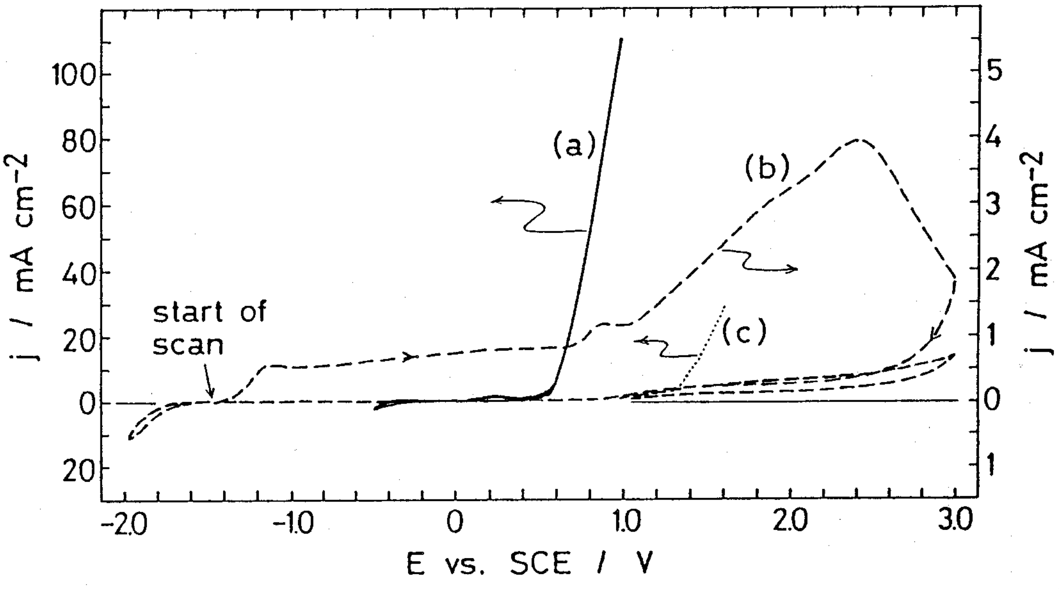

Fig. 8 Cyclic voltammograms for ZrN_x (a), Zr metal (b), and a carbon plate (c), in 1.0 M KOH at room temperature. The current density scales are different between curves (a) and (b). The scan rate is 50 mV/s.

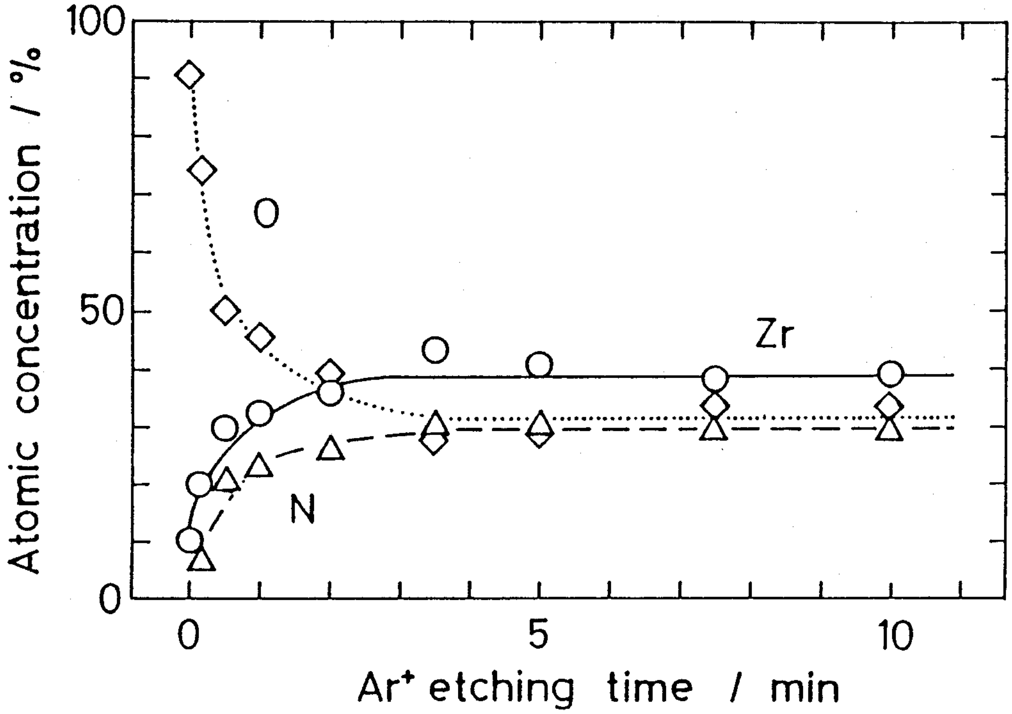

Fig. 9 A depth profile of the ZrN_x film deposited on a carbon substrate measured after passing 2.4 C cm^{-2} (20 mA cm^{-2}, 120 s) of oxygen evolution current in 0.5 M H_2SO_4.

oxidized when it made a contact with an aqueous solution.

The electrocatalytic activity of the NbN_x and the ZrN_x electrodes for the oxygen evolution reaction strongly depended on the pH of the solutions. Namely, the onset potentials of the oxygen evolution currents for these electrodes in 0.5 M H_2SO_4 or 0.5 M Na_2SO_4 were about 0.3 V more positive than that for a smooth Pt electrode in each solution, but were 0.4 V more negative in 1.0 M NaOH than that for Pt. Figure 10 shows the OH^--concentration dependence of the oxygen evolution current densities for the ZrN_x electrode at a constant overvoltage η, i.e., at potentials more positive than the calculated thermodynamic oxygen evolution potentials by a constant value η. It is seen that the reaction rate increases with the OH^- concentration rather linearly. Similar results were obtained for the NbN_x electrode.

Figure 11 shows a Tafel plot for the oxygen evolution on the ZrN_x electrode (○) in 1.0 M KOH, measured under a quasi-steady-state galvanostatic condition, compared with those for smooth platinum (◇) and smooth nickel (△) electrodes. Good linearity was obtained for ZrN_x in a region of 5×10^{-4} to 5×10^{-2} A cm^{-2}. The deviation from the linearity at low current densities is due to a contribution from an oxidation current in the carbon-substrate surface, which is probably caused by the penetration of the electrolyte solution through cracks or pin-holes of the ZrN_x film to the substrate. The Tafel plot in Fig. 11 indicates that

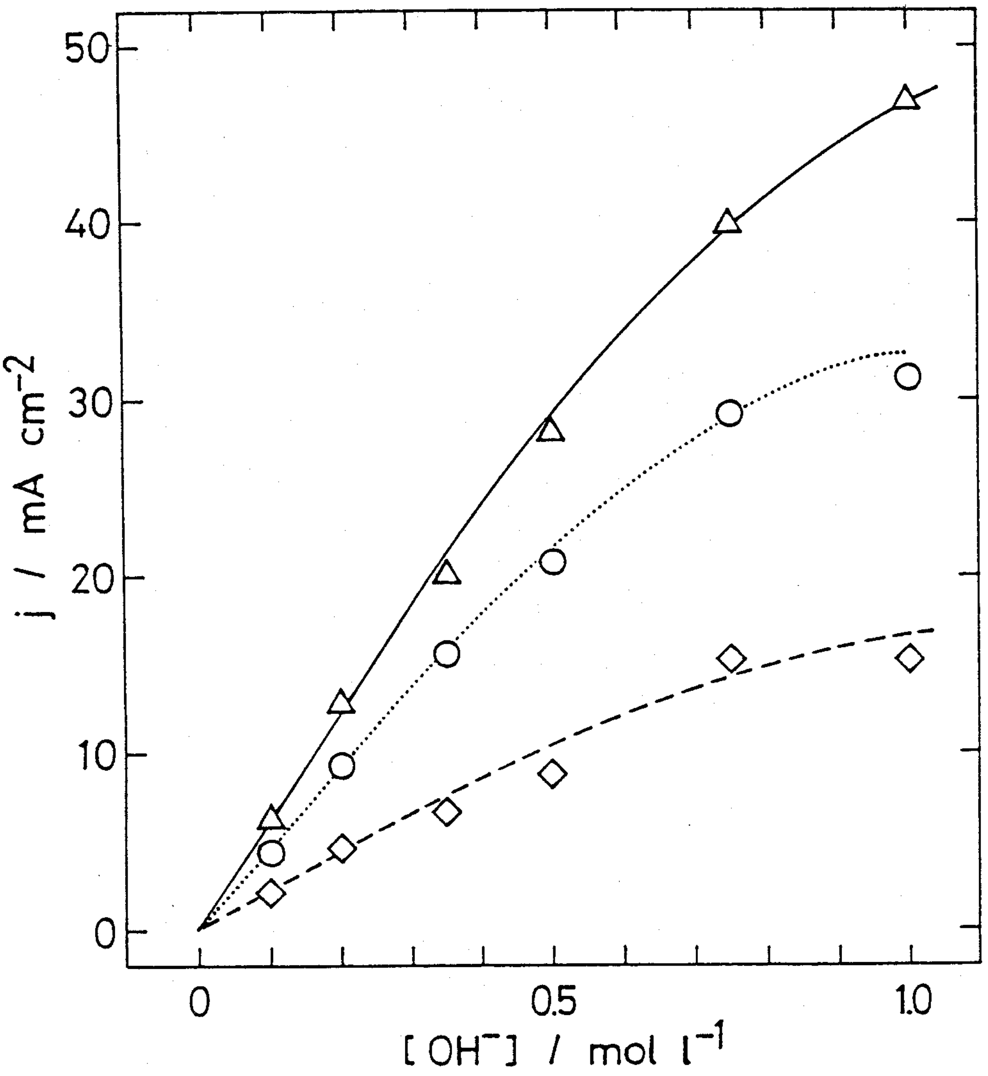

Fig. 10 Dependence of oxygen evolution current densities in the ZrN_x electrode on the OH^- concentrations at fixed overpotentials, η = 0.8 V (solid line), 0.7 V (dotted line) and 0.6 V (broken line). The solutions are prepared by mixing 1.0 M NaOH and 0.5 M Na_2SO_4 solutions.

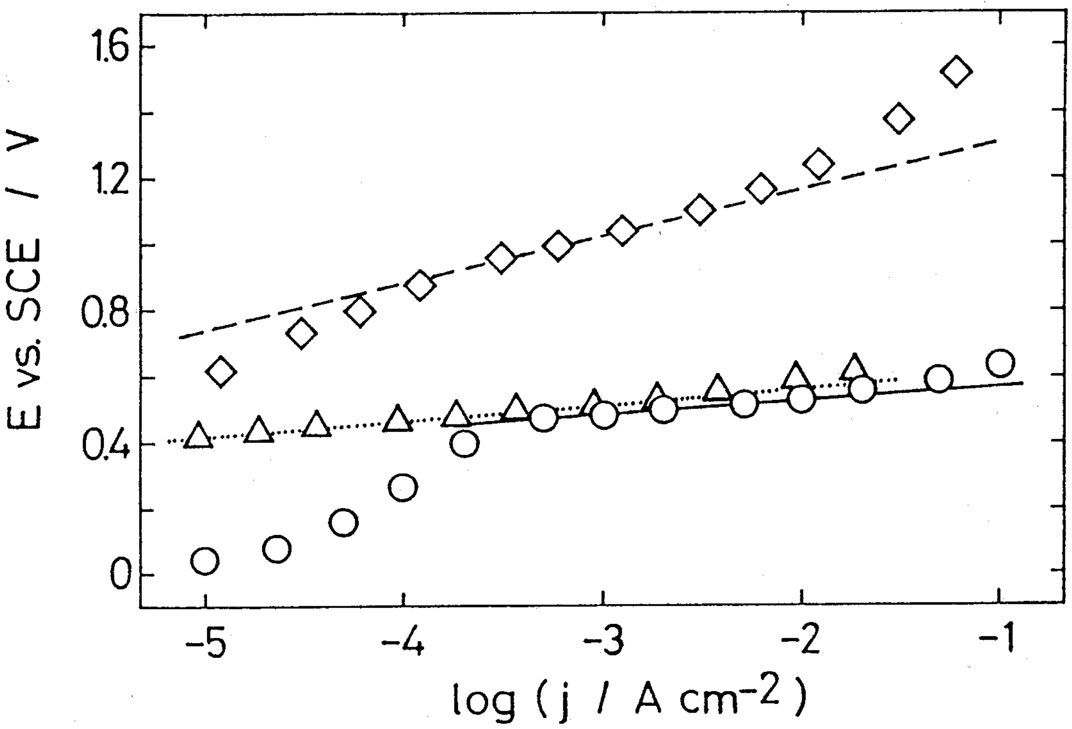

Fig. 11 Tafel plots for the oxygen evolution currents at a ZrN_x film electrode (solid line), smooth platinum (broken line) and smooth nickel (dotted line) electrodes in 1.0 M KOH at room temperature. The i-R drop is not corrected.

the ZrN_x electrode in an alkaline solution has the electrocatalytic activity for the oxygen evolution nearly the same as or even slightly higher than that for a smooth nickel electrode, though detailed comparison should be made after correction for the roughness factors (R) of the electrodes. The R value for the ZrN_x films was estimated to be 5 to 20 times as large as that for smooth platinum, by comparing cyclic voltammograms for the $Fe(CN)_6^{3-}/Fe(CN)_6^{4-}$ redox reaction as proposed by Theodoridou et al. [14]. A similar value was obtained for the NbN_x films. These R value should, however, be taken as giving the upper limit because they should include a contribution of current at naked carbon surfaces probably present inside the carbon substrate as is expected from Fig. 1.

Exchange current densities (j_0) and Tafel slopes determined from the Tafel plots are summerized in Table 1. The exchange current densities for the NbN_x and ZrN_x electrodes are scattered in a fairly wide range, depending on specimens, but it is likely that they are larger than those for Pt and Ni even after correction for the roughness factors, suggesting that the oxygen evolution reactions on NbN_x and ZrN_x are faster than on Pt and Ni. The Tafel slopes for NbN_x and ZrN_x were, however, larger than that for Ni.

Both the NbN_x and ZrN_x electrodes were inactive for the oxidation of methanol and the reduction of oxygen, but caused stable evolution of chlorine in HCl or NaCl solutions. Figure 12

Table 1 Exchange current densities (j_0) and Tafel slopes for the oxygen evolution in 1.0 M KOH.

Electrode	log (j_0 / A cm^{-2})	Tafel slope / mV dec^{-1}
ZrN_x	-5.8 ± 1.0	90 - 150
NbN_x	-7.8 ± 2.0	50 - 90
Pt	- 9.2	100 - 150
Ni	-11.5	30 - 60

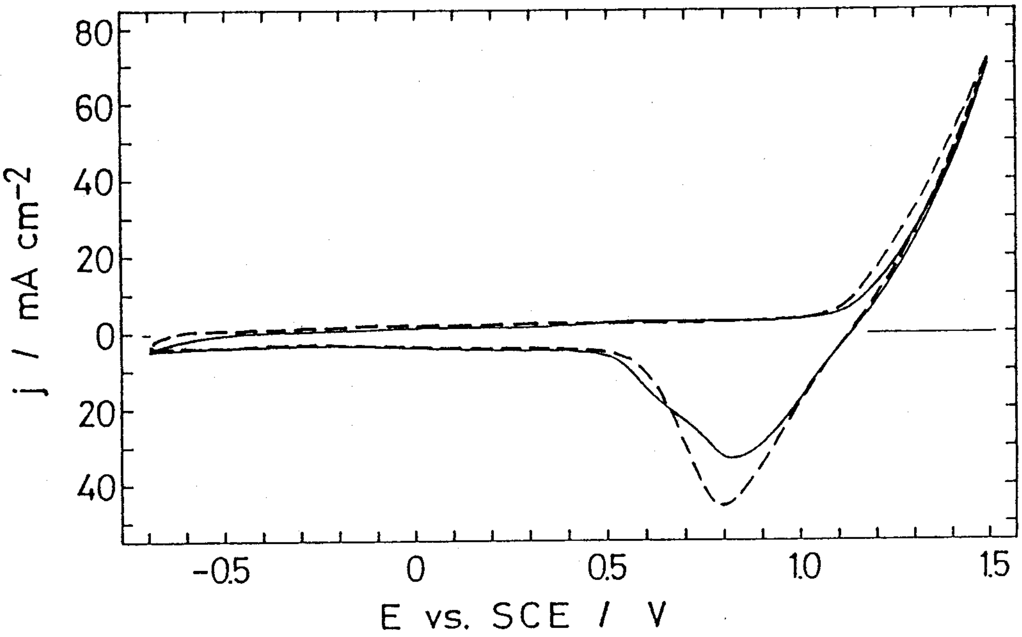

Fig. 12 Current(j)-potential(E) curves for chlorine evolution on NbN$_x$ (solid line) and carbon (dotted line) electrodes in 3.0 M NaCl at room temperature. The scan rate is 50 mV/s.

shows a current(j)-potential(E) curve for the NbN_x electrode in 3.0 M NaCl, compared with that for a carbon electrode. These two electrodes gave similar j-E curves, indicating that they have similar catalytic activity.

The NbN_x or ZrN_x films were sometimes peeled off from the carbon substrates during long-term experiments of the oxygen evolution. Figure 13 shows the potential vs. time for an NbN_x electrode when the oxygen evolution current was kept at 100 mA cm^{-2}. The potential started to shift toward the positive in about 30 min, probably due to partial peeling-off of the NbN_x film from the substrate. It is likely that, since the NbN_x film has many cracks or pin-holes as is expected from Fig. 1, the electrolyte solution can penetrate through these cracks or pin-holes to the underlying carbon substrate, and the oxygen evolution reaction can occur near the interface between the carbon and nitride layers, finally causing the peeling off of the films.

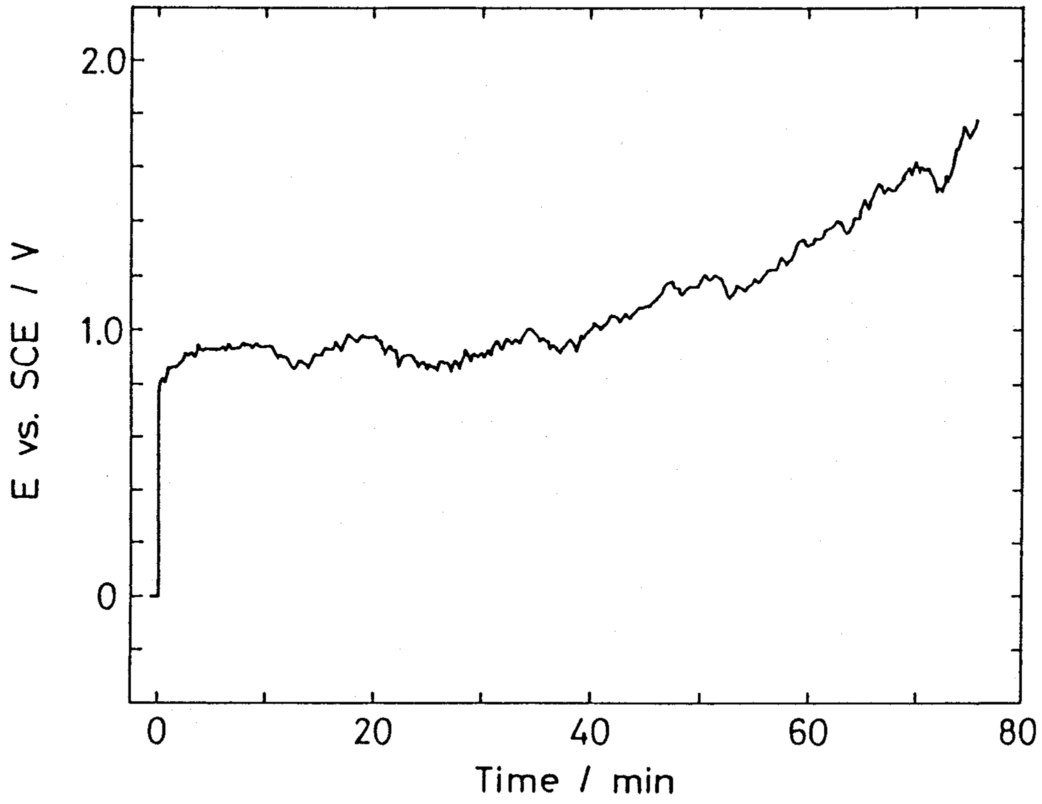

Fig. 13 The electrode potential of an NbN_x electrode vs. time under the galvanostatic oxygen evolution at 100 mA cm^{-2}.

Discussion

The XPS studies showed that the NbN_x films just deposited were covered with thin oxide layers (Figs. 3 (a) and 4) when they were exposed to air probably due to oxidation by air. The thickness of the surface oxide layers was estimated to be about 2 to 3 nm. The ZrN_x films just deposited (Figs. 5 (a) and 6) were covered with about 1-nm thick oxide layers, thinner than those for the NbN_x films. But these oxide layers for ZrN_x became thicker, to about 5 nm, when the films were in contact with aqueous solutions (Fig. 5 (c)). It is important to note that the surface oxide layers for both the NbN_x and the ZrN_x films no longer grew by prolonged flow of the oxygen evolution current (Figs. 3 (d), 5 (d), and 9), quite contrary to the cases of Nb and Zr metals. The reason why these nitrides form no thick (passivating) oxide layers will be discussed in Chapter 2.

The above-mentioned fact that the surface oxide layers for NbN_x and ZrN_x did not grow thicker explains the sustained evolution of oxygen observed (Figs. 7 and 8). Figure 14 schematically shows the chemical structure near the surface of the NbN_x electrode. The oxygen evolution reaction must be initiated by the oxidation of surface OH or O^- group in the surface oxidized layer. Since this layer is very thin as mentioned above and probably porous, the OH or O^- group lie rather close to the nitride/oxide interface, and their oxidation (i.e., electron transfer from the OH or O^- species into the NbN_x

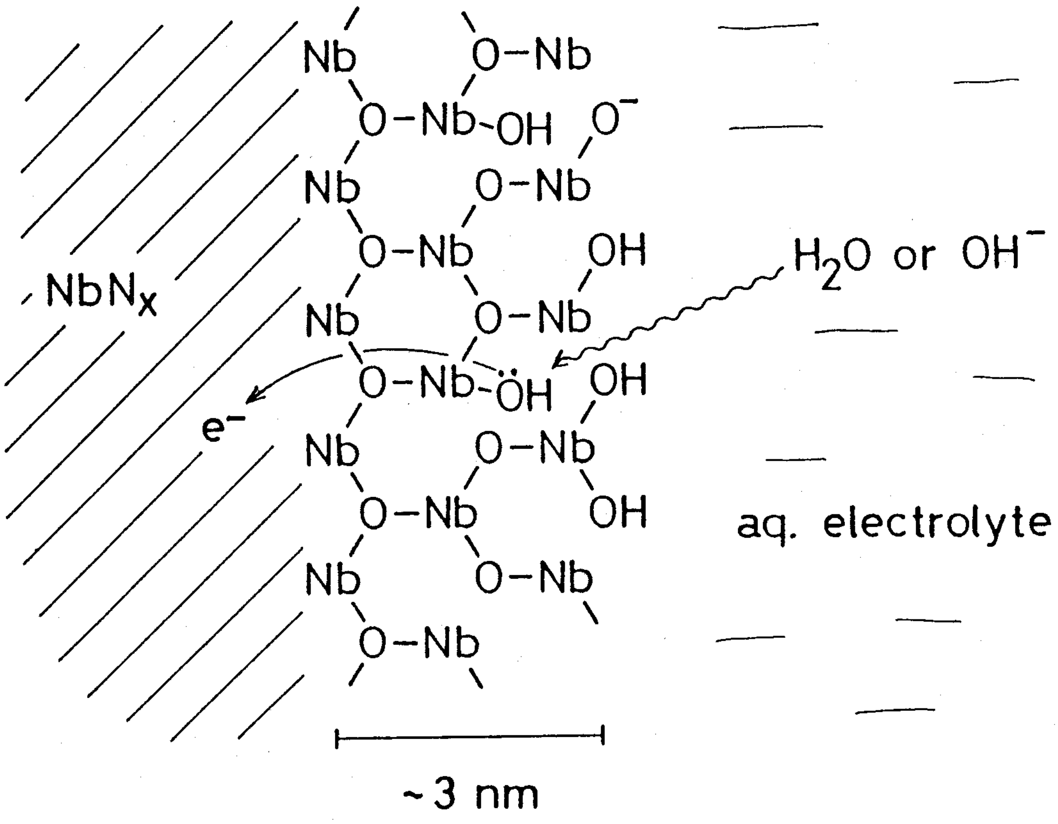

Fig. 14 Schematic illustration of NbN$_x$-electrolyte interface.

layer) is expected to occur by quantum-mechanical tunneling (Fig. 14).

The oxygen evolution on the NbN_x or the ZrN_x films become quite efficient with increasing OH^- concentration in the solution (Fig. 10). A possible explanation for this is given on the basis of the model of Fig. 14 as follows: The surface OH group, denoted by M-OH (M = Nb or Zr), in the surface oxidized layer will be in an acid-base equilibrium with the solution,

$$\text{M-OH} \rightleftharpoons \text{M-O}^- + \text{H}^+$$

The resulting deprotonated $M-O^-$ species will be oxidized much more easily than the protonated M-OH species, or in other words, the redox potential for the oxidation of the former species should be considerably more negative than that for the latter. This assumption is supported by a mechanism for the oxygen photoevolution reaction on an n-type titanium dioxide ($n-TiO_2$, rutile) electrode, proposed by us from photo- and electroluminescence studies [15]. Accordingly, as the pH goes up, the concentration of the $M-O^-$ species will increase and the oxygen evolution efficiency will be enhanced. The linear increase in the current density with the OH^- concentration (Fig. 10) suggests that the concentration of $M-O^-$ increases linearly with the OH^- concentration. This implies that the negative charge accumulation due to the deprotonation is compensated by the diffusion of positive ions (e.g. Na^+) from the solution into the layer, as well as the electronic polarization of the nitride film because the oxide layer is thin and porous (Fig. 14).

The NbN_x and the ZrN_x film electrodes were inactive for the oxidation of methanol and the reduction of oxygen, but fairly active for the oxidation of Cl^- ions (Fig. 12). These results can be explained also on the basis of Fig. 14 by assuming that the bond between the metal and the OH or O^- group is so strong that neither methanol nor oxygen molecules can be substituted for these groups. The methanol and oxygen molecules which are outside the surface oxidized layers of the nitride films cannot react with the electrode efficiently. For the case of Cl^-, on the other hand, it can be assumed that the Cl^- ions can be substituted for the OH group due to the similarity of their chemical properties, as follows:

$$M\text{-}OH + Cl^- \longrightarrow M\text{-}Cl + OH^-$$

This explains the activity of the nitride electrodes for the Cl^- oxidation.

In conclusion, the present work has revealed that both the NbN_x and the ZrN_x films are stable, only covered with very thin oxide layers even under higher anodic potentials, and can cause efficient oxygen evolution in alkaline solutions. These results are significant in that active electrode materials for the oxygen evolution have been found in the compounds not containing VIII-A group transition metals.

References

1. I. I. Vasilenko, N. N. Nechiporenko and D. M. Bubai, Chem. Abst., 75 (1971) 115240u.
2. N. Tamari and A. Kato, Denki Kagaku (English), 44 (1976) 477.
3. Y. Matsuda, M. Inoue, M. Morita, Y. Takasu, H. Mizuno and H. Miura, Denki Kagaku (English), 50 (1982) 258.
4. M. Morita, Y. Yonehara, Y. Matsuda, H. Mizuno and H. Miura, Denki Kagaku (English), 50 (1982) 755.
5. M. Morita, F. Tachihara, Y. Matsuda and H. Mizuno, Denki Kagaku (English), 53 (1985) 504.
6. M. Azuma, Y. Nakato and H. Tsubomura, Mater. Res. Bull., 22 (1987) 527.
7. M. Azuma, Y. Nakato and H. Tsubomura, J. Electroanal. Chem., 220 (1987) 369.
8. M. Azuma, Y. Nakato and H. Tsubomura, submitted to J. Electroanal. Chem.
9. D. E. Hall, J. Electrochem. Soc., 132 (1985) 41c.
10. S. Trasatti and W. E. O'Grady in H. Gerisher and C. W. Tobias (Ed.), Advances in Electrochemistry & Electrochemical Engineering, vol. 12, Wiley Interscience, New York, 1981, p. 177.
11. B. MacDougall, D. F. Mitchell and M. J. Graham, J. Electrochem. Soc., 132 (1985) 2895.
12. ASTM card, 6-0719.
13. ASTM card, 2-0956.

14. E. Theodoridou, J. O. Besenhard and H. P. Fritz, J. Electroanal. Chem., 124 (1981) 87.
15. Y. Nakato, H. Ogawa, K. Morita and H. Tsubomura, J. Phys. Chem., 90 (1986) 6210.

Chapter 2.

High Electrochemical Stability of Zirconium- and Niobium-Nitride Amorphous Films in Sharp Contrast to Unstable Titanium- and Vanadium-Nitrides.

Summary

The electrochemical stability of transition-metal nitride amorphous thin films (TiN_x, VN_x, ZrN_x and NbN_x), prepared by the reactive RF sputtering technique on carbon substrates, was investigated in aqueous electrolyte solutions. TiN_x films, as well as Ti metal, were rapidly passivated under anodic polarization. VN_x films and V metal rapidly dissolved in solutions. These properties are in sharp contrast to those of ZrN_x and NbN_x films, reported previously by us to be stable and evolve oxygen and chlorine. XPS studies showed that TiN_x films (and also Zr and Nb metals) were covered with thick oxide layers after anodic treatment, while ZrN_x and NbN_x films were covered only with very thin oxide layers (a few nanometers or less) after anodic processes. The above difference in the electrochemical stability among the four nitrides showed no correlation with the difference in melting points and mechanical hardness. Also, the difference could not be explained by the thermodynamic decomposition potentials. A tentative explanation is given by

taking account of matching between the distance of M-N bonds in the nitride films and that of M-O bonds in the oxide overlayers.

Introduction

Transition metal nitrides such as TiN, VN, ZrN and NbN have attracted much attention for their excellent properties such as hardness, high melting points and metallic conductivity. These properties indicate that the chemical bonds between transition metals and nitrogen are strong. Studies have been made on the electrochemical properties of some transition metal nitrides such as TiN [1-4], VN [3], NbN [5] and TaN [5]. These studies have shown that such transition metal nitrides are unstable like the respective metals themselves under anodic polarization, i.e., they are either passivated (TiN [3], NbN [5] and TaN [5]) or dissolved into aqueuos solutions (VN [3]). In these studies, the nitrides were prepared in the form of polycrystalline films either by the thermal nitridation of metal plates or by the chemical vapor deposition on metal substrates, and little attention was paid to the passivation of the underlying metal substrates which may be caused by the penetration of electrolyte solutions through cracks or pin-holes of the nitride films to the substrates.

We have investigated the electrochemical properties of several transition-metal nitride films (TiN_x, VN_x, ZrN_x and NbN_x) deposited on stable carbon substrates by the reactive RF sputtering technique, and recently reported that niobium- and zirconium-nitride (NbN_x and ZrN_x) films were electrochemically stable in aqueous solutions of pH from zero to 14, causing oxygen and chlorine evolution [6-8], contrary to the results reported by other workers [1-5]. The electrocatalytic activity of the NbN_x and the ZrN_x electrodes for the oxygen evolution in alkaline solutions was as high as or even slightly higher than that for a smooth nickel electrode which is known as an efficient and low-cost material for water electrolysis. These findings imply that the nitridation of transition metals improves their electrochemical properties. This is interesting because only a limited number of materials (mostly expensive noble matals or their compounds) are known to be stable in a wide range of pH, and cause oxygen evolution. Carbon is chemically stable, but causes swelling under prolonged hydrogen or oxygen evolution due to the intercalation of these gases.

In Chapter 1, we reported the results of our detailed studies with emphasis on the high electrocatalytic activity of the ZrN_x and the NbN_x films for the oxygen evolution in alkaline solutions. In this chapter, we will compare the stability of various transition metal nitrides (TiN_x, VN_x, ZrN_x and NbN_x) under anodic polarization, and discuss their stability in connection with the results of XPS studies on the surface chemical structure [9].

Experimental

Transition-metal nitride films were deposited on carbon substrates (Kyowa Carbon, 2 mm thick) by the reactive RF sputtering technique. The details of our method were described in Chapter 1. Titanium nitride (TiN_x) and vanadium nitride (VN_x) were prepared using Ti and V metal plates (Furuuchi Chemicals, 99.9 %) as targets. All the nitrides (TiN_x, VN_x, ZrN_x and NbN_x) were deposited by discharge under a 4 to 10 x 10^{-1} Pa nitrogen atmosphere for 3 h at an RF power of 2.5 W cm^{-2}. The average thickness of the deposited films was calculated to be 0.70 ± 0.07 μm for TiN_x, 0.50 ± 0.05 μm for VN_x, 0.70 ± 0.07 μm for ZrN_x and 0.90 ± 0.10 μm for NbN_x, from the weight increase and the specific gravities for these nitrides assumed to be 5.4, 6.1, 7.32 and 5.43 g cm^{-3}, respectively.

The morphology of the nitride films was investigated with an Akashi-Seisakusho ALPHA 30 A scanning electron microscope (SEM), and the crystal structure was investigated with a Shimadzu VD-1 X-ray diffractometer (XRD). The surface chemical composition was analyzed by the X-ray photoelectron spectroscopy (XPS) with a Shimadzu ESCA 750 spectrometer. Depth profiles were obtained by combining the XPS with the Ar^+-ion sputtering technique. The binding energies were corrected by using the C 1s peak at 285.00 eV for contaminating carbon or the Au $4f_{7/2}$ peak at 83.80 eV for gold vacuum-deposited on the sample edge, as the standard.

Electrochemical measurements were made with a commercial potentiostat and function generator. Further details were described in Chapter 1.

Results

1. Characterization of Titanium- and Vanadium-Nitride Films.

Scanning electron micrographs of the TiN_x and VN_x films deposited on carbon substrates showed that they covered the surface carbon particles uniformly, as described in Chapter 1 for the ZrN_x films [8]. No fine particle structure was observed even at high magnification, contrary to the case of NbN_x films [7].

Figure 1 (a) shows an X-ray diffraction (XRD) pattern for a TiN_x film deposited on a quartz plate. No diffraction peak was observed in a range of the diffraction angle (2θ) from 34° to 45°, though commercial crystalline TiN (cubic) powder showed clear peaks at 36.7° and 42.8° (pattern c). The TiN_x film showed weak peaks after thermal treatment at 1000°C for 20 min under a nitrogen atmosphere (pattern b), indicating that the deposited film crystallized to some extent by this thermal treatment. The XRD pattern for the TiN_x films deposited on carbon substrates was the same as Fig. 1 (a) except that it exhibited some peaks ascribable to the crystalline carbon substrate. These results indicate that the TiN_x films deposited in the present work are amorphous or at least in the form of microcrystals of several nanometers or less in size. The VN_x films also showed no XRD peak in a range of 2θ from 18° to 83°.

Figure 2 shows XPS spectra for Ti 2p and N 1s peaks for a TiN_x film deposited on a smooth Si substrate. Spectra (a) is for an as-deposited specimen (no Ar^+-ion etching), and spectra (b)

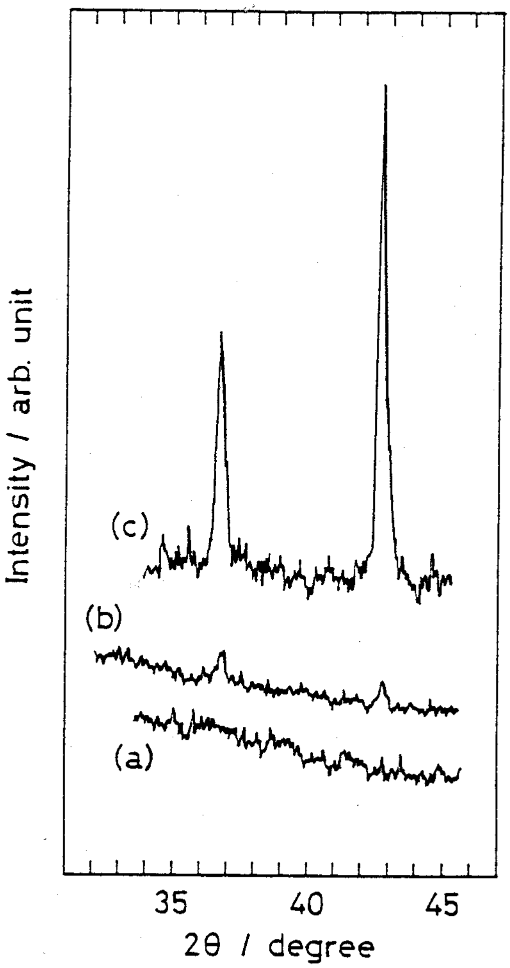

Fig. 1 X-ray diffraction (XRD) patterns; (a) for a TiN_x film (0.70 μm thick) sputter-deposited on a quartz plate, (b) after thermal treatment at 1000°C for 20 min under a nitrogen atmosphere, and (c) for crystalline TiN (cubic) powder.

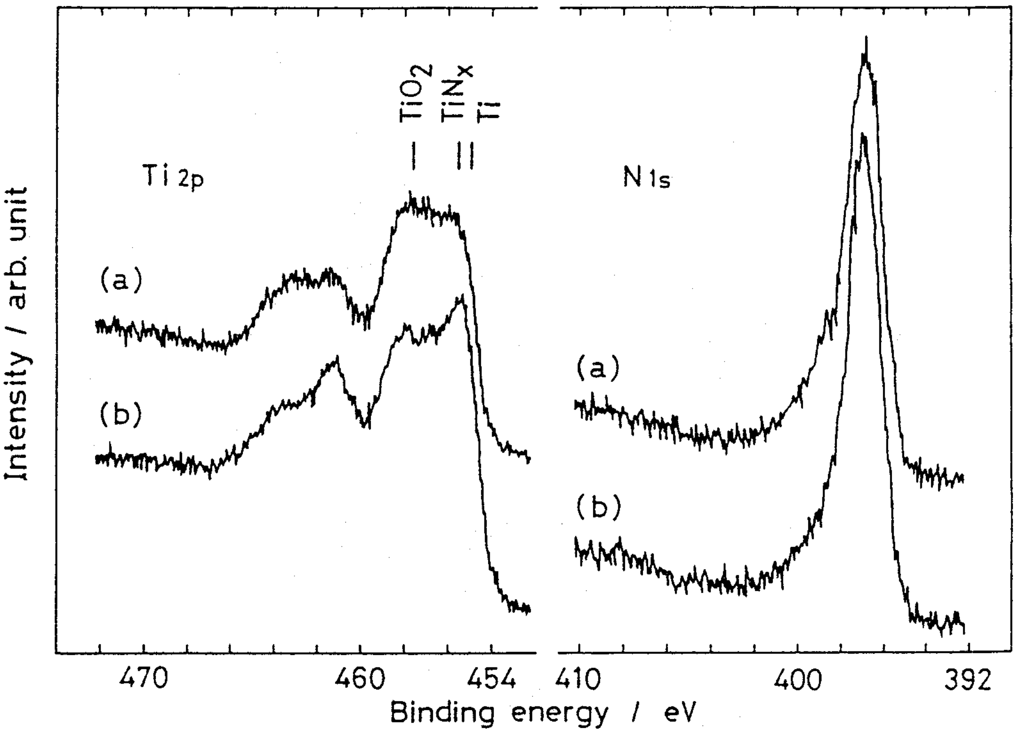

Fig. 2 XPS spectra for Ti 2p and N 1s peaks for a TiN$_x$ film sputter-deposited on a smooth Si wafer: (a) for no Ar$^+$-ion etching and (b) after 30-s Ar$^+$-ion etching.

was measured after 30 s of Ar^+-ion etching. Spectra (b) were no longer changed by further etching. The spectrum assignable to the Ti $2p_{3/2}$ and $2p_{1/2}$ peaks in the region from 454 to 466 eV can be divided into four peaks. In them, two peaks at 457.6 and 463.3 eV can be assigned to the Ti peaks of the oxide because they coincide with the peaks appearing in TiO_2 prepared by thermal oxidation of a Ti metal plate in air. They are stronger in spectrum (a) than spectrum (b). The remaining two peaks at 455.2 and 461.2 eV can therefore be assigned to the Ti peaks of the nitride. The two oxide peaks (or shoulders) in spectrum (b) were much stronger than the corresponding peaks in other nitrides (ZrN_x, NbN_x and VN_x) (cf. Fig. 4), indicating that the TiN_x film either has a high oxygen concentration or is easily oxidized by contaminating oxygen under the XPS measurements. The high intensity of the oxidized Ti in spectrum (a) indicates that the surface of the as-deposited TiN_x film is oxidized. The thickness of this oxide layer is roughly estimated to be a few nanometers by assuming that the Ar^+-ion sputter rate for the titanium oxide is the same as that for SiO_2, 10 nm min^{-1}. The intensity for the N 1s peak is enhanced by the Ar^+-ion etching (Fig. 2).

Figure 3 shows relative atomic concentrations (A.C.) for the TiN_x film as a function of the Ar^+-ion etching time, together with the binding energies for the N 1s and the Ti $2p_{3/2}$ peaks. The (N/Ti) atomic ratio was about 1.2 at the surface (i.e., for no Ar^+-ion etching), but it gradually decreased with the Ar^+-ion

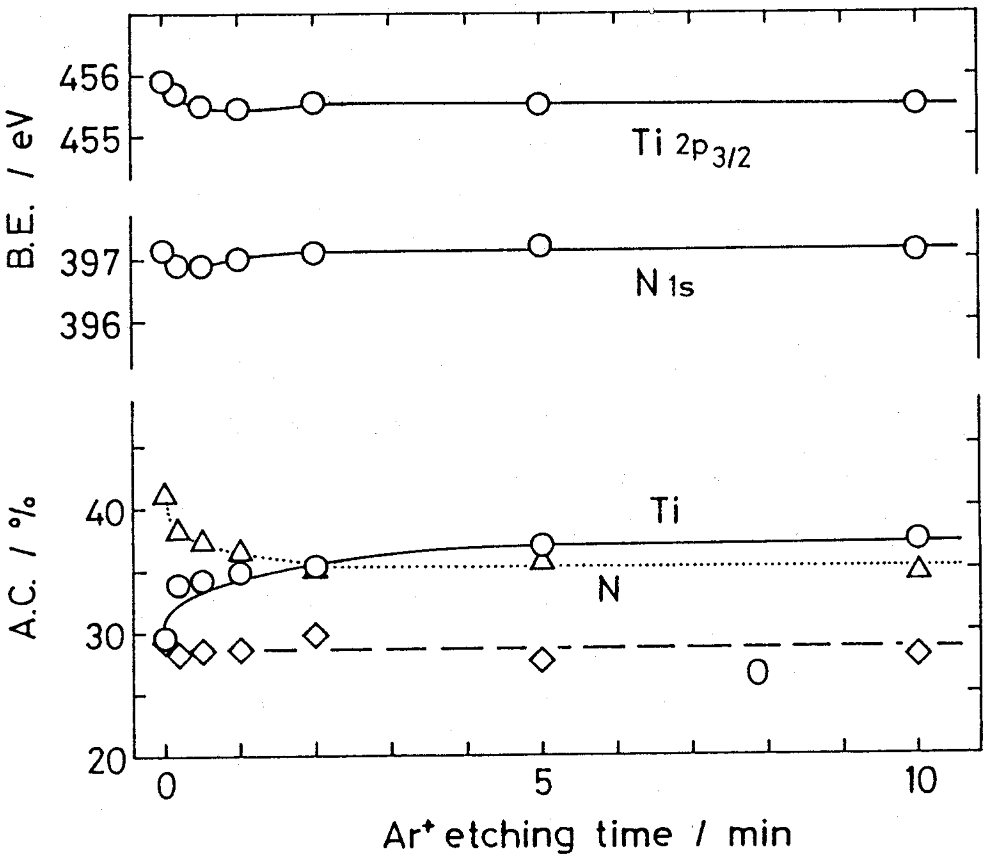

Fig. 3 Relative atomic concentrations (A.C.) for the same TiN_x film as shown in Fig. 2 as a function of the Ar^+-ion etching time, together with the binding energies for the N 1s and the Ti $2p_{3/2}$ peaks.

etching time, finally attaining a constant value of 0.90 ± 0.10 in a region of the etching time longer than 1 min. This ratio is not corrected for the (unknown) difference in the sputter rates between Ti and N. In the present study, the titanium nitride films of the above chemical composition is designated as TiN_x, as was done for NbN_x and ZrN_x in the previos chapter [7,8]. The shift of the binding energy for the Ti $2p_{3/2}$ peak in the etching time from 0 to 0.5 min (Fig. 3) indicates the removal of the oxide layer by the Ar^+-ion etching. The binding energy for the Ti $2p_{3/2}$ peak was 0.6 eV higher than that for Ti metal, but 2.2 eV lower than that for TiO_2. The binding energy of the N 1s shifted very little with the Ar^+-ion etching.

Figure 4 shows XPS spectra for V 2p and N 1s peaks for a VN_x film deposited on a Si substrate. Spectrum (b), measured after the 10-s Ar^+-ion etching, was no longer changed by further etching, indicating that it was for the VN_x film. Namely, the peak at 513.80 eV can be assigned to the V $2p_{3/2}$ peak for VN_x. The V $2p_{1/2}$ peak for VN_x is at ca. 520 eV and is not shown in Fig. 4. Vanadium oxide prepared by thermal oxidation of the V metal showed a V $2p_{3/2}$ peak at 516.00 eV. Accordingly, the weak shoulder at 516 eV in spectrum (b) indicates that a small amount of oxygen is present in the VN_x film. Spectrum (a) for no Ar^+-ion etching showed the V $2p_{3/2}$ peak for VN_x at 513.80 eV and a clear shoulder at about 516 eV, indicating that the surface of the as-deposited VN_x film was somewhat oxidized. The thickness of

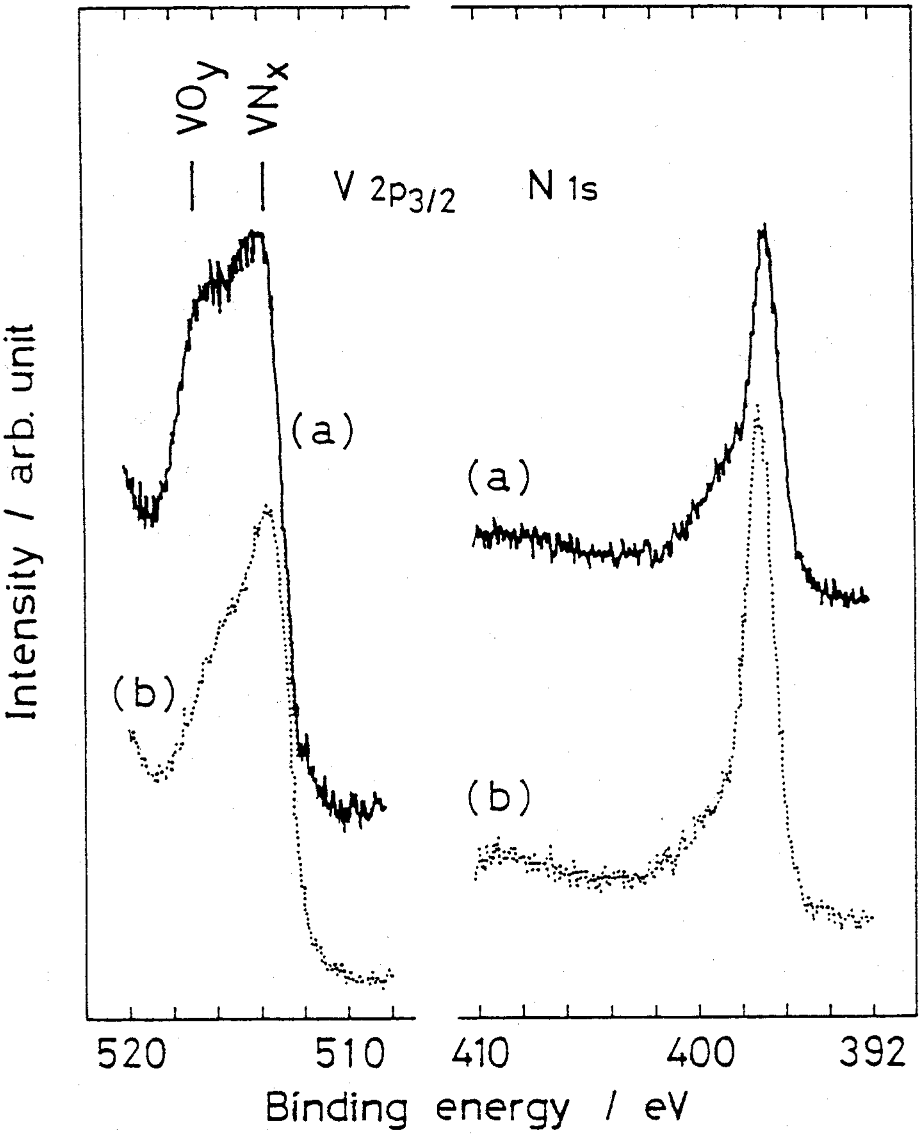

Fig. 4 XPS spectra for V 2p and N 1s peaks for a VN_x film sputter-deposited on a smooth Si wafer: (a) for no Ar^+-ion etching and (b) after the 10-s Ar^+-ion etching.

this oxide layer was roughly estimated to be 1 nm or less by assuming that the Ar^+-ion etching rate for the vanadium oxide was 10 nm min^{-1}.

Figure 5 shows relative atomic concentrations for the VN_x film, together with the binding energies for the N 1s and the V $2p_{3/2}$ peaks, in the same way as in Fig. 3. The (N/V) atomic ratio was 2.00 ± 0.20 at the surface (for no Ar^+-ion etching), and 1.50 ± 0.10 in a region of the etching time longer than 10 s. This (N/V) ratio is not corrected for the difference in the sputter rate between V and N, as mentioned above for the TiN_x film. The film of the above composition is designated as VN_x. The binding energy of the V $2p_{3/2}$ peak for the VN_x film was 0.75 eV higher than that for V metal, but 2,5 eV lower than that for vanadium oxide.

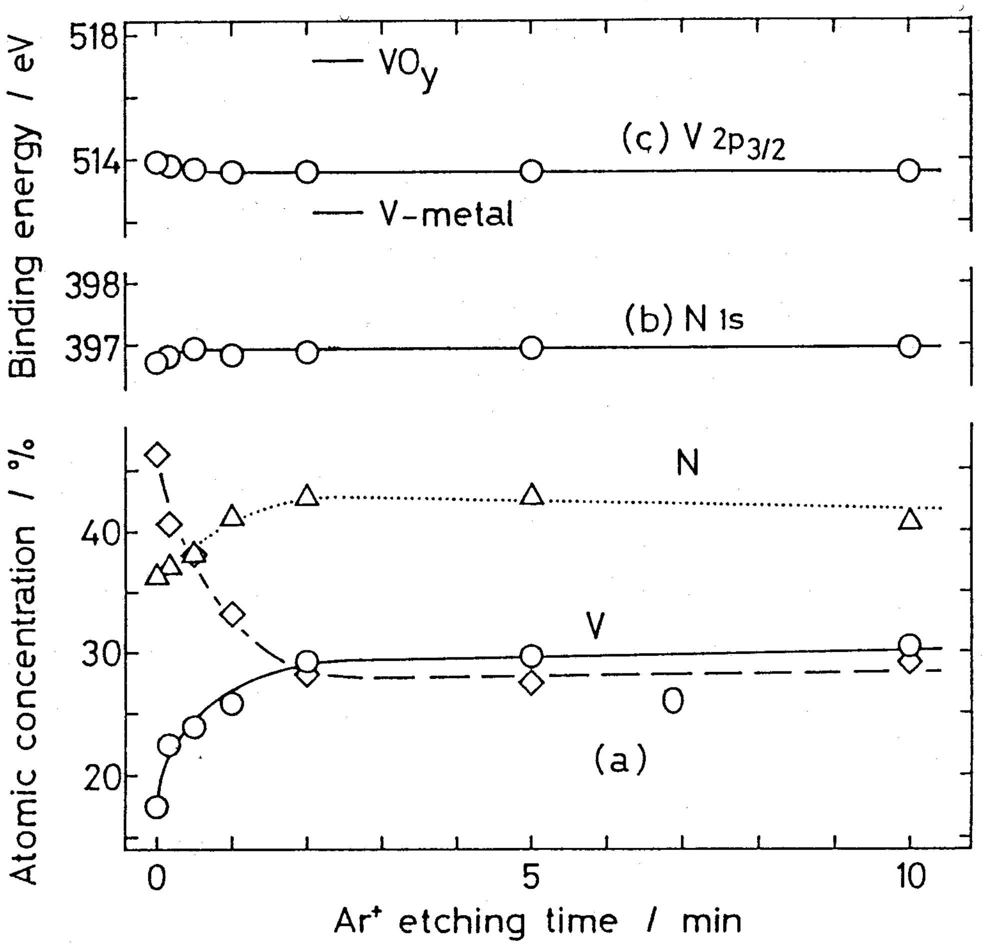

Fig. 5 Relative atomic concentrations (A.C.) for the same VN_x film as shown in Fig. 4 as a function of the Ar^+-ion etching time, together with the binding energies for the N 1s and the V $2p_{3/2}$ peaks.

2. Electrochemical Properties of TiN_x and VN_x Films.

In Fig. 6, curve a shows a typical cyclic voltammogram for a TiN_x film electrode in 0.5 M H_2SO_4, and curve b for a Ti metal electrode in the same solution. The anodic current for the Ti metal electrode was observed only in the first forward (negative to positive) scan, indicating that this anodic current is due to the oxidation (passivation) of the Ti metal electrode. The anodic current for the TiN_x film was also observed only in the first forward scan, indicating that the TiN_x film was passivated. A similar result was reported by Matsuda et al. [3]. The onset potential for the passivation current in the first forward scan for the TiN_x film was 0.8 to 1.3 V more positive than that for the Ti metal electrode.

Figure 7, curve a shows a cyclic voltammogram for a VN_x film electrode in 0.5 M H_2SO_4, compared with that for a V metal electrode (curve b). The anodic current for the V metal electrode, rising at about 0.3 V vs. SCE, was due to the dissolution of the V metal electrode [10]. The anodic current for the VN_x electrode started to flow at ca. 0.5 V, arose rather sharply with the potential, reached a peak at about 1.2 V, and decreased rapidly. This anodic current was accompanied by the vigorous gas evolution. The cyclic voltammograms in the backward and later scans were nearly the same as those of the carbon substrate electrode suggesting that the VN_x layer dissolved rapidly. XPS measurements showed that no vanadium nitride was

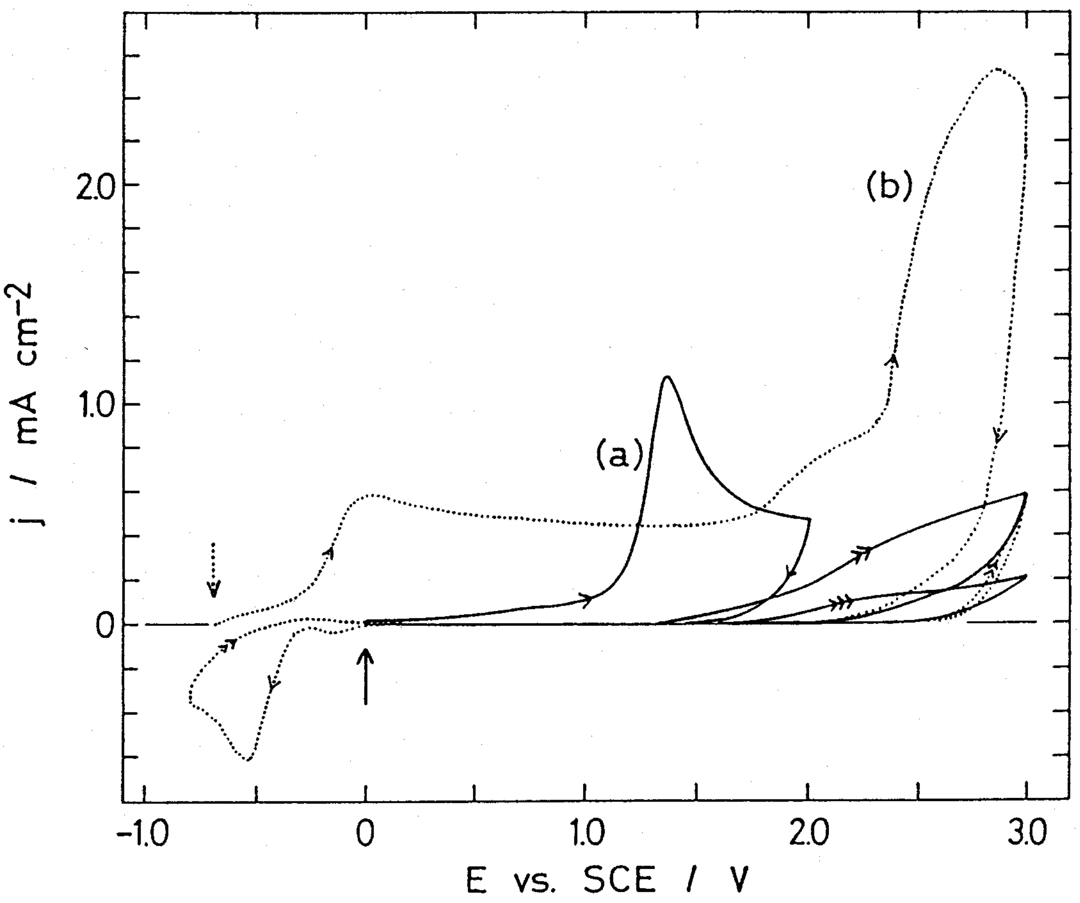

Fig. 6 Cyclic voltammograms in 0.5 M H_2SO_4: (a) For a TiN_x electrode. (b) That for a Ti metal electrode. The potential sweep was started at points marked by arrays. The sweep rate was 50 mV/s.

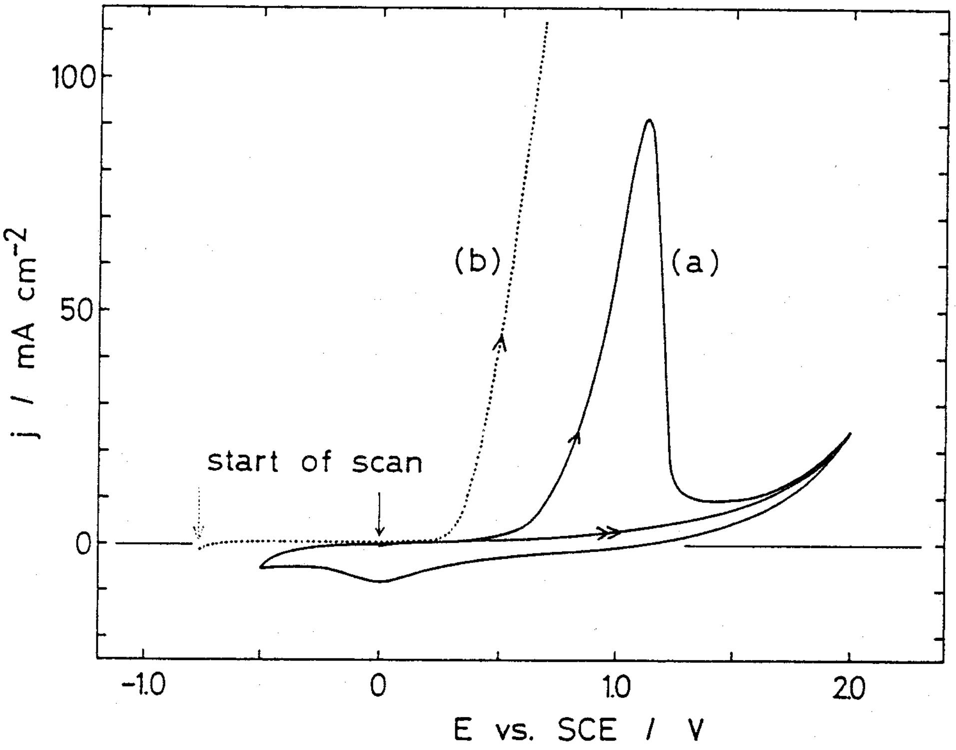

Fig. 7 Cyclic voltammograms in 0.5 M H_2SO_4: (a) For a VN_x electrode. (b) That for a V metal electrode. The potential sweep was started at points marked by arrays. The sweep rate was 50 mV/s.

left at the electrode surface after this measurement. These results indicate that the anodic current for the VN_x film is caused by its dissolution into the solution, forming vanadium cations and nitrogen molecules.

We reported in Chapter 1 [6-9] that the ZrN_x and NbN_x film electrodes were electrochemically stable, causing steady oxygen or chlorine evolution under anodic polarization, though Zr and Nb metals were passivated and showed no steady anodic current. Figure 8 (b) shows an Nb 3d XPS spectrum for an Nb metal electrode, measured after the flow of an anodic (passivation) current of 300 μA cm^{-2} for 100 s in 0.5 M H_2SO_4, compared with spectrum (a) for a fresh Nb metal electrode etched in 5% HF for several seconds. Spectrum (b) agreed with that of niobium oxide prepared by thermal oxidation in air, showing that the Nb metal electrode was covered with rather thick oxide layer by the flow of the anodic current.

Figure 9 (A) shows a depth profile for the Nb metal electrode that gave the XPS spectrum (b) in Fig. 8. The formation of an oxide layer having a constant atomic (O/Nb) ratio of 5/2 (probably Nb_2O_5) is clearly seen in a region of the Ar^+-ion etching time from 0.5 to 2 min (Fig. 9(A)). The thickness of this oxide layer was roughly estimated to be ca. 20 nm by assuming that the sputter rate for Nb_2O_5 was the same as that for SiO_2, 10 nm min^{-1}. Figure 9 (B) is for an NbN_x film electrode in which an oxygen evolution current of 10 mA cm^{-2} was passed for 200 s in

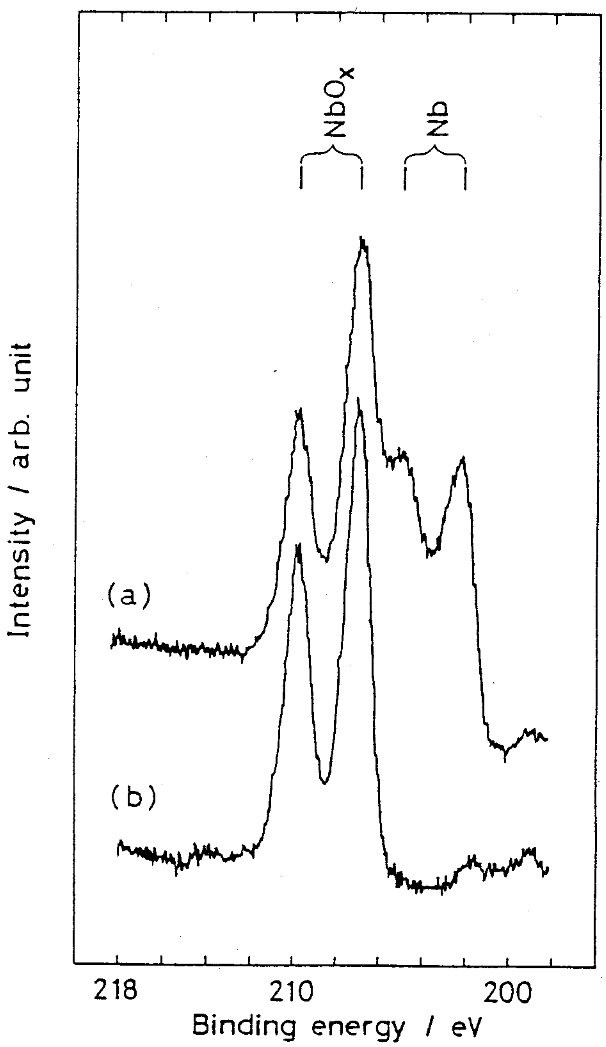

Fig. 8 (a) Nb 3d XPS specta for a fresh Nb metal electrode etched in 5% HF for several seconds. (b) That for the same electrode as (a) except that an anodic current of 300 μA cm^{-2} was passed for 100 s in 0.5 M H_2SO_4.

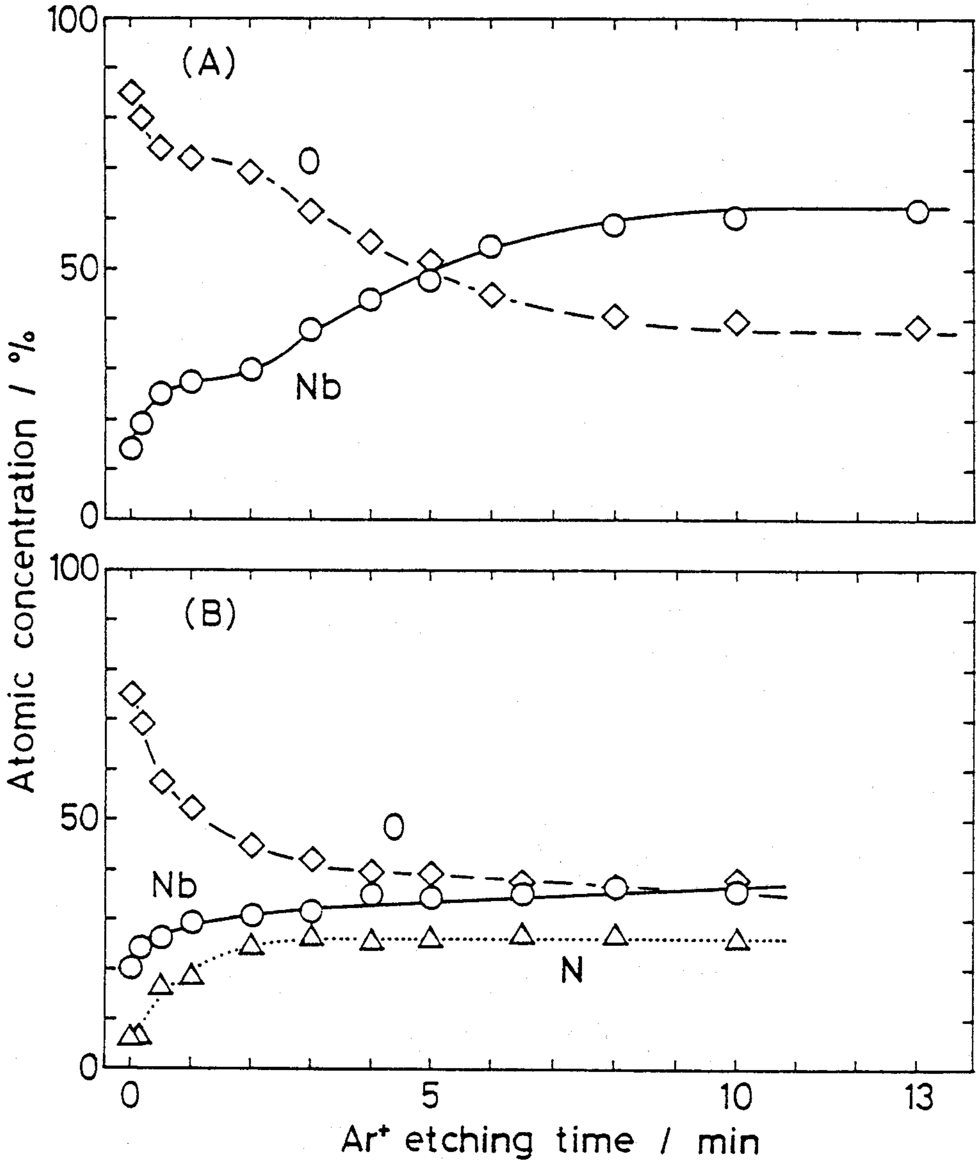

Fig. 9 (A) The depth profiles for the Nb metal electrode that gave the spectrum (b) in Fig. 8. (B) That for an NbN_x film electrode in which an oxygen evolution current of 10 mA cm^{-2} was passed for 200 s in 0.5 M H_2SO_4.

0.5 M H_2SO_4. It shows that the NbN_x film electrode is also oxidized at the surface (Fig. 9(B)), but the Nb and O concentrations changed rather sharply in a region of the short Ar^+-ion etching time, indicating that the oxide layer formed is thin. The thickness of the oxide layer was estimated in Chapter 1 to be about a few nanometers or less [8]. Similar results were obtained for the Zr metal and the ZrN_x electrodes.

Discussion

As described in the preceding section, the TiN_x and the VN_x films under anodic potentials are either passivated or dissolved into electrolyte solutions, whereas the ZrN_x and the NbN_x films are quite stable, causing oxygen and chlorine evolution. What is the reason for such a difference in the electrochemical stability between these nitrides? To clarify this reason is important for elucidating the key factors to derive new stable and efficient electrode materials.

It was reported by Naka et al. that amorphous metal-matalloid and metal-metal alloys exhibited higher corrosion-resistance than polycrystalline alloys of the same composition. They concluded [11] that amorphous alloys were corrosion-resistant due to their chemically homogeneous single-phase nature which resulted in the formation of uniform protective passive films. Although the NbN_x and ZrN_x films in the present work are amorphous as mentioned before, these nitrides are stable without forming any thick protective passive films, contrary to the above reported cases. It is thus difficult to explain the stability of these nitrides as being due to their amorphous structure. This argument is supported by the fact that the amorphous TiN_x and VN_x films are not stable.

The first and second columns of Table 1 show the melting points and mechanical hardness reported for the crystalline transition-metal nitrides of the cubic structure [12]. These

Table 1. Melting points and hardness for transition-metal nitrides together with the smallest atomic distances d(M-N) in nitrides MN (cubic, NaCl-type) and d(M-O) in oxides MO (cubic, NaCl-type).

Nitride	Melting Point(°C)	Hardness (kg mm^{-2})	d(M-N) (nm)	d(M-O) (nm)	Δd (nm)
TiN	2949[a]	2000[a]	0.2122[b]	0.2090[b]	0.0032
VN	2177[a]	1500[a]	0.2064[c]	0.2031[c]	0.0033
ZrN	2982[a]	1500[a]	0.2163[d]	0.2163[d]	0.0000
NbN	2204*,[a]	1400[a]	0.20956[e]	0.21051[e]	-0.00095

* decomposition

a: Ref. 12, b: Ref. 13, c: Ref. 14, d: Ref. 15, e: Ref. 16

quantities must have certain correlation with the bond strength in the transition-metal nitrides. The melting points for the nitrides of IV-A group metals (Ti and Zr) are somewhat higher than those for the V-A group metals (V and Nb). The hardness of the TiN is higher than those of the other nitrides. Thus, there are no correlation between these properties and the observed electrochemical stability.

Table 2 summarizes the observed binding energies for the main XPS peaks for the transition metals together with their shifts by the formation of the nitrides and oxides. The positive shifts $\Delta E_{nitride}$ by the nitride formation indicate that the metal atoms in the nitrides are positively polarized. The shifts by the nitride formation for ZrN_x and NbN_x are somewhat larger than those for TiN_x and VN_x, showing a correlation with the electrochemical stability. However, this difference in $\Delta E_{nitride}$ is related with the electronegativity of the metals, and cannot explain directly the observed high stability for the ZrN_x and NbN_x films.

Figure 10 shows thermodynamic redox potentials ε_d for the oxidation reactions of the crystalline transition-metal nitrides MN (M = Ti, V, Zr or Nb, cubic structure) at pH = 0, described as follows:

$$MN + x\,H_2O \longrightarrow MO_x\ (\text{or } M^{z+}) + 1/2\ N_2 + 2x\ H^+ + 2x\ e^-$$

Table 2. Observed binding energies for the main XPS peaks for the transition metals and their chemical shifts by the formation of the amorphous nitrides and oxides.

XPS peak	binding energy	$\Delta E_{nitride}$	ΔE_{oxide}
Ti $2p_{3/2}$	454.80 ± 0.20	0.60 ± 0.40	2.80 ± 0.40
V $2p_{3/2}$	512.80 ± 0.10	0.75 ± 0.20	3.20 ± 0.10
Zr $3d_{5/2}$	179.50 ± 0.20	1.40 ± 0.40	3.60 ± 0.50
Nb $3d_{5/2}$	203.20 ± 0.20	1.30 ± 0.40	4.30 ± 0.40

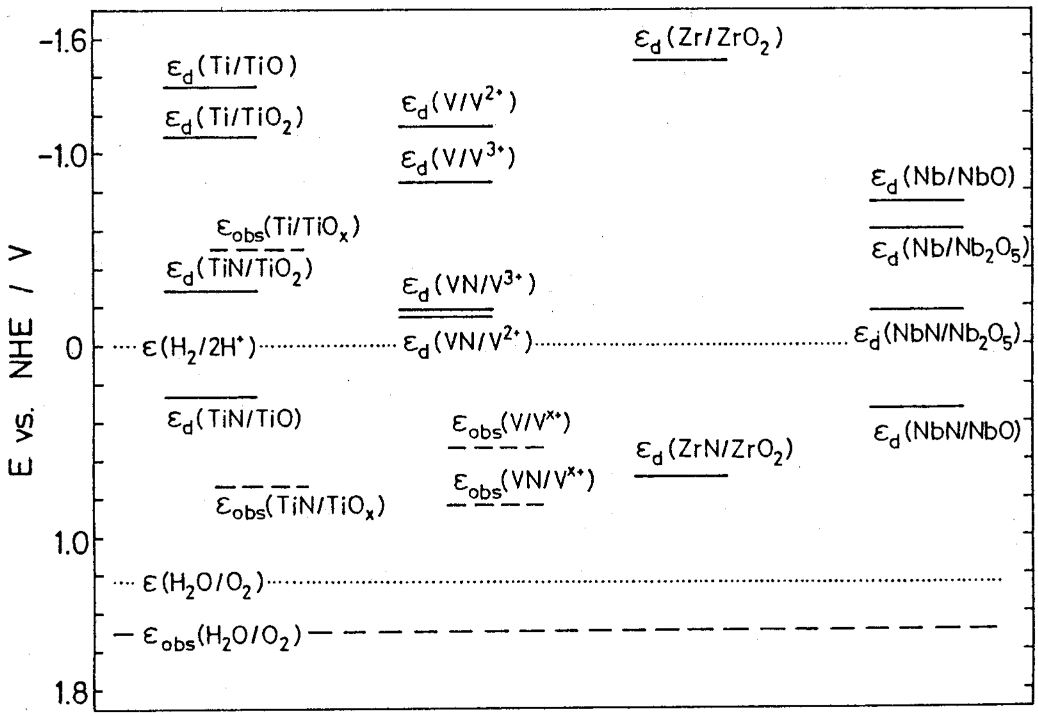

Fig.10 Thermodynamic redox potentials for some oxidation reactions of the crystalline transition-metal nitrides (cubic) at pH 0, compared with those for the oxidation reactions of the respective metals. $\varepsilon(H_2/2H^+)$ and $\varepsilon(H_2O/O_2)$ are the thermodynamic hydrogen and oxygen evolution potentials, respectively. ε_{obs} is the observed onset potential for the anodic current corresponding to the oxidation of the metal or metal-nitride electrodes.

The ε_d values for these reactions, abbreviated as MN/MO_x or MN/M^{z+} in Fig. 10, were calculated from the Gibbs energies of formation for the reactants and products [14]. The ε_d values for the oxidation of metals (M),

$$M + x\ H_2O \longrightarrow MO_x\ (\text{or } M^{z+}) + 2x\ H^+ + 2x\ e^-$$

are also included in Fig. 10 for reference, together with the thermodynamic hydrogen and oxygen evolution potentials, $\varepsilon(H_2/2H^+)$ and $\varepsilon(H_2O/O_2)$.

The ε_d values for the metal nitrides thus calculated and given in Fig. 10 are considerably more positive than those for the respective metals. This indicates that the metal nitrides are more stable against oxidation than the metals. The ε_d values for all the nitrides are yet more negative than $\varepsilon(H_2O/O_2)$. This means that all the nitrides should be unstable for oxygen evolution, in disagreement with the experimental results for ZrN_x and NbN_x. The ε_d value for TiN is nearly the same as that for NbN, though the electrochemical stability observed for TiN_x is quite different from that of NbN_x. Accordingly, it is difficult to explain the difference in the electrochemical stability by the thermodynamic consideration. This conclusion is not essentially changed by taking account of other oxidation reactions, e.g., reactions producing nitrogen oxides instead of nitrogen molecules.

In Fig. 10, the observed onset potential ε_{obs} for the anodic currents corresponding to the oxidation of the metal and metal-nitride electrodes are also included. Because the ZrN_x and NbN_x films cause stable oxygen evolution, the ε_{obs} values for these nitrides must be more positive than the observed oxygen evolution potential $\varepsilon_{obs}(H_2O/O_2)$. Therefore, the differences between ε_{obs} and ε_d for these nitrides are much larger than those for TiN_x and VN_x. This means that the activation energies for the oxidation reactions of the ZrN_x and NbN_x electrodes are higher than those of other metal nitrides. It is worthwhile to point out here that, for both cases of the ZrN_x and NbN_x films, the surface oxide layers formed during prolonged anodic oxygen evolution reaction are very thin (a few nanometers or less) [8]. This implies that the growth of the oxide layers on these nitrides is quickly suppressed, while for the TiN_x or metal electrodes the oxide layers grow more extensively (cf. Fig. 9A).

A tentative explanation for this can be given by taking account of the difference between the metal-nitrogen distances d(M-N) for the nitrides and the metal-oxygen distances d(M-O) in the oxide layers. In Table 1 are listed the d(M-N) values reported of the crystalline nitrides (MN, cubic) and the d(M-O) values of the oxides (MO, cubic). The differences Δd between d(M-N) and d(M-O) for ZrN and NbN are much smaller than those for TiN and VN, suggesting that the ZrN and NbN films are covered with oxide layers having good lattice matching with the nitrides.

This means that the metal-nitrogen bond at the interface between the ZrN or NbN film and the respective oxide layer is less distorted than the M-N bond at the TiN/TiO interface or the meatl-metal bond at metal/oxide interfaces. After the nitride was covered with a very thin oxide layer, further oxide growth must proceed along with the diffusion of either OH^- or H_2O through the oxide layer into the nitride surface or the metal cations of the nitride surface through the oxide layer out onto the oxide surface. Therefore, in either case, the oxide formation reaction should involve the break down of the metal-nitrogen bond and hence need a higher activation energy for the case of ZrN and NbN than the case of TiN. (For the case of VN, anodic dissolution occurs faster than the oxygen evolution.) It might also be possible that the oxide layer is less compact for the case of TiN as well as metal electrodes, so that the diffusion of reactive species through the oxide layer is faster than the case of ZrN and NbN. Thus, for the case of ZrN and NbN, the occurrence of the oxygen evolution reaction prevents further growth of the oxide layer.

In conclusion, the present work has revealed that some of the transition-metal nitrides are stable against oxidation much more than expected from thermodynamic predictions. It is tentatively suggested that good lattice matching at the interface between the nitride and the oxide overlzyer gives rise to a large activation energy for the growth of the oxide layer, leading to high electrochemical stability of the nitride electrodes.

References

1. I. I. Vasilenko, N. N. Nechiporenko and D. M. Bubai, Chem. Abst., 75 (1971) 115240u.
2. N. Tamari and A. Kato, Denki Kagaku (English), 44 (1976) 477.
3. Y. Matsuda, M. Inoue, M. Morita, Y. Takasu, H. Mizuno and H. Miura, Denki Kagaku (English), 50 (1982) 258.
4. M. Morita, Y. Yonehara, Y. Matsuda, H. Mizuno and H. Miura, Denki Kagaku (English), 50 (1982) 755.
5. M. Morita, F. Tachihara, Y. Matsuda and H. Mizuno, Denki Kagaku (English), 53 (1985) 504.
6. M. Azuma, Y. Nakato and H. Tsubomura, Mater. Res. Bull., 22 (1987) 527.
7. M. Azuma, Y. Nakato and H. Tsubomura, J. Electroanal. Chem., 220 (1987) 369.
8. M. Azuma, Y. Nakato and H. Tsubomura, submitted to J. Electroanal. Chem.
9. M. Azuma, Y. Nakato and H. Tsubomura, submitted to J. Electroanal. Chem.
10. Y. Israel and L. Meites in A. J. Bard (Ed.), Encyclopedia of Electrochemistry of the Elements, vol. 7, Marcel Dekker, New York, 1976, p 293.
11. M. Naka, K. Hashimoto and T. Masumoto, J. Non-Cryst. Solids, 30 (1978) 29.
12. L. E. Toth, Transition Metal Carbides and Nitrides, Academic Press, New York (1971).

13. V. A. Gubanov, E. Z. Kurmaev and G. P. Shveikin, J. Phys. Chem. Solids, 38 (1977) 201.

14. The Japan Chemical Society (Ed.), Kagaku Binran (Kiso-hen), vol. 2, Maruzen (1975).

15. A. L. Ivanovsky, V. P. Zhukov V. A. Gubanov and G. P. Shveikin, J. Phys. Chem. Solids, 41 (1980) 1333.

16. M. Gupta, V. A. Gubanov and D. E. Ellis, J. Phys. Chem. Solids, 38 (1977) 499.

Chapter 3.

Reduction of Oxygen to Water on Cobalt Nitride Thin Film Electrodes Prepared by the Reactive RF Sputtering Technique.

Summary

Electrochemical reduction of oxygen was carried out on amorphous cobalt-nitride (Co_xN) thin film electrodes, prepared by the reactive RF sputtering technique. The onset potential of the oxygen reduction current in the Co_xN electrode in neutral electrolyte solutions was close to that on a platinum metal electrode which are known to be the most efficient material for the oxygen reduction. Measurements with rotating-disk-electrodes (RDE) and rotating-ring-disk-electrodes (RRDE) showed that oxygen reduction into water (the four-electron-transfer type) proceeded in the Co_xN electrodes, contrary to Co metal electrodes which caused only two-electron-transfer type reduction into hydrogen peroxide. The reason for improved electrocatalytic activity by nitridation is discussed.

Introduction

Electrochemical oxygen reduction is an important reaction in view of energy conversion and storage; for example, in fuel cells. This reaction can be divided into two types: One is the reduction of oxygen into water (four-electron-transfer type), which is reported to occur on a limited number of metal electrodes [1] such as platinum, palladium and silver, and on carbon electrodes coated with tetrasulfonated iron phthalocyanine (Fe-TsPc) [2] and covalently-linked (face-to-face) cobalt porphyrin dimers (abbreviated as face-to-face Co-Co-4 porphyrins in the literatures) [3-7]. The other is the reduction into hydrogen peroxide (two-electron-transfer type), which is reported to occur on most other metal electrodes [8] such as gold, cobalt and iron, and on cobalt-phthalocyanine modified electrode [9]. The four-electron-transfer type is desirable from the view-point of the energy conversion. For both the types of reactions, the overpotential at current densities in practical systems (ca. a few mA cm^{-2}) are 0.3 to 0.5 V. To reduce this high overpotential is important from the standpoint of efficient energy conversion.

Many studies have been made in search of low-cost and efficient electrode materials for the oxygen reduction [8,9]. However, no material that is more active than platinum has been reported yet. Very recently, Vante et al. reported that $Mo_{4.2}Ru_{1.8}Se_8$ had fairly high activity for the four-electron-transfer type oxygen reduction [10].

As mentioned above, transition metals such as Co and Fe are known to show only poor electrocatalytic activity for the oxygen reduction of the two-electron-transfer type [8]. On the contrary, complexes of these transition metals with N_4-chelates such as porphyrin, phthalocyanine and tetraazaanulen are reported to show fairly high catalytic activity [8,9], though these complexes, except face-to-face Co-Co-4 porphyrin and Fe-TsPc, can only cause the two-electron-transfer type reduction. These results might suggest that Co atoms surrounded by several nitrogen atoms have high electrocatalytic activity for the oxygen reduction.

Recently, we have studied the electrochemical properties of transition metal nitrides such as TiN_x, VN_x, ZrN_x and NbN_x, and reported [11-14] that the ZrN_x and NbN_x electrodes are electrochemically stable in solutions of a wide pH range (Chapter 2) and cause fairly efficient oxygen and chlorine evolution (Chapter 1), quite contrary to the respective metals (Zr and Nb) which are easily passivated. In this chapter we will report that cobalt nitride (Co_xN) thin film electrodes cause the four-electron-transfer type oxygen reduction [15], contrary to the cobalt metal electrodes.

Experimental

Cobalt-nitride (Co_xN) films were deposited on smooth titanium metal (99.6%) plates as substrates by the reactive RF sputtering technique, using a cobalt plate (Furuuchi Chemicals, 1 mm thick, 99.9 %) as a target. Details on our sputtering apparatus were given in Chapter 1. The titanium substrates were chemically etched in 5% HF, rinsed, degreased by immersing in acetone, and further sputter-etched by nitrogen plasma in the sputtering apparatus for more than 30 min. The Co_xN films were then sputter-deposited on the Ti plates thus cleaned, under about 1.0×10^{-2}-Torr nitrogen atmosphere (1 Torr = 133.3 Pa) for 2 h at an RF power of 2.5 W cm^{-2}. The average thickness of the deposited film was calculated to be 1.72 ± 0.18 μm from the weights of the films with the specific gravities assumed to be 9.0 g cm^{-3}.

The surface morphology of the deposited films was inspected with an Akashi-Seisakusho ALPHA 30 A scanning electron microscope (SEM), and the crystallinity was investigated with a Shimadzu VD-1 X-ray diffractometer (XRD).

Depth profiles were obtained with a Shimadzu ESCA 750 X-ray photoelectron spectrometer (XPS), combined with the Ar^+-ion sputter-etching technique. The binding energies were corrected by taking the C 1s peak of contaminating carbon at 285.00 eV as the standard.

The Co_xN electrodes for electrochemical measurements were prepared in a way, as described in Chapter 1. They were etched in 3 M HCl (M = mol dm^{-3}) for several seconds before the measurements. In addition to electrodes for measurements under static conditions, rotating disk Co_xN electrodes (RDE) and rotating ring (Pt)-disk (Co_xN) electrodes (RRDE) were used together with a Nikko Keisoku model RRDE-1 system and a model DPGS-1 dual potentiogalvanostat. Oxygen reduction currents were studied at room temperature, passing oxygen or nitrogen bubble in the solution. A saturated calomel electrode (SCE) and a Pt-plate electrode were used as the reference and the counter electrodes, respectively. Electrolyte solutions were prepared using analytical grade chemicals and water purified with a Japan Millipore Corp. Milli-Q Water Purification System.

Results

1. Characterization of Sputter-Deposited Co_xN Films. A scanning electron micrograph of a Co_xN film deposited on a Ti metal substrate showed that the nitride covered the entire Ti surface, though some cracks were present (Fig. 1). No XRD peak was observed in a range of the diffraction angle (2θ) from 20° to 100°, indicating that the Co_xN films prepared in the present work were amorphous, as descrived previously by us for nitrides of Ti, V, Zr and Nb [13,14].

Figure 2 shows XPS spectra for Co 2p and N 1s where (a) is for no Ar^+-ion sputter etching and (b) is after 30-s Ar^+-ion etching. Spectrum (b) was not changed by further etching, indicating that it is truly for the Co_xN bulk. Two peaks at 778.4 and 793.6 eV can be assigned to the Co $2p_{3/2}$ and $2p_{1/2}$ peaks, respectively. Spectrum (a) showed another peak at about 781 eV, which coincides with the Co $2p_{3/2}$ peak of cobalt oxide. This indicates that the surface of the Co_xN film is slightly oxidized. The thickness of the oxide layer was estimated to be 1 to 2 nm by assuming that the Ar^+-ion etching rate is the same as that for SiO_2, 10 nm min^{-1}. The intensity of the N 1s peak was somewhat enhanced by the Ar^+-ion etching (Fig. 2).

Figure 3 shows relative atomic concentrations for the Co_xN film as a function of the Ar^+-ion etching time, together with the binding energies for the N 1s and Co $2p_{3/2}$ peaks. The atomic ratio (Co/N) was constant, about three in a region of the Ar^+-ion

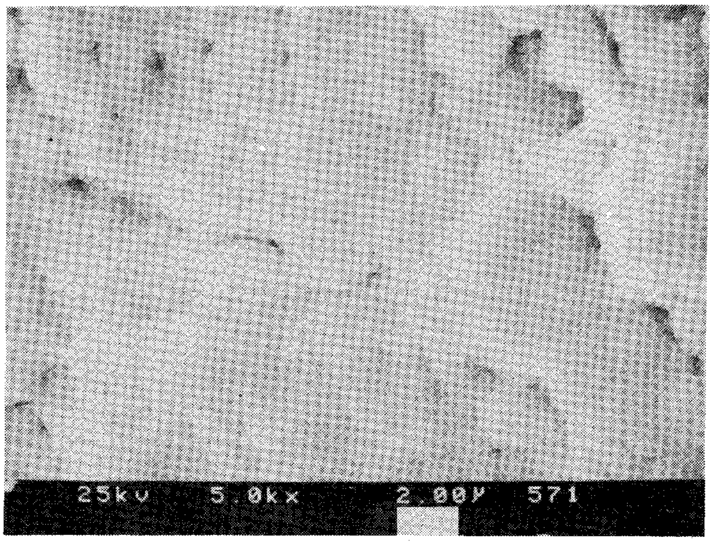

Fig. 1 Scanning electron micrograph of a Co_xN film (1.9 μm thick) deposited on a Ti metal substrate.

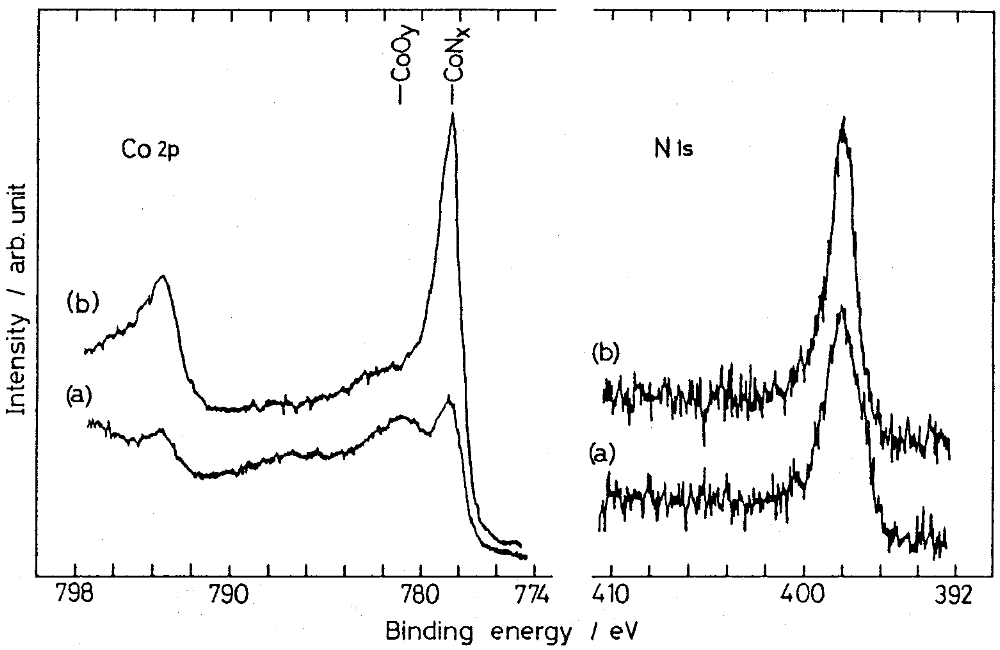

Fig. 2 XPS spectra for Co 2p and N 1s peaks for a Co_xN film deposited on a smooth Si wafer: (a) for no Ar^+-ion etching and (b) after the 30-s Ar^+-ion etching.

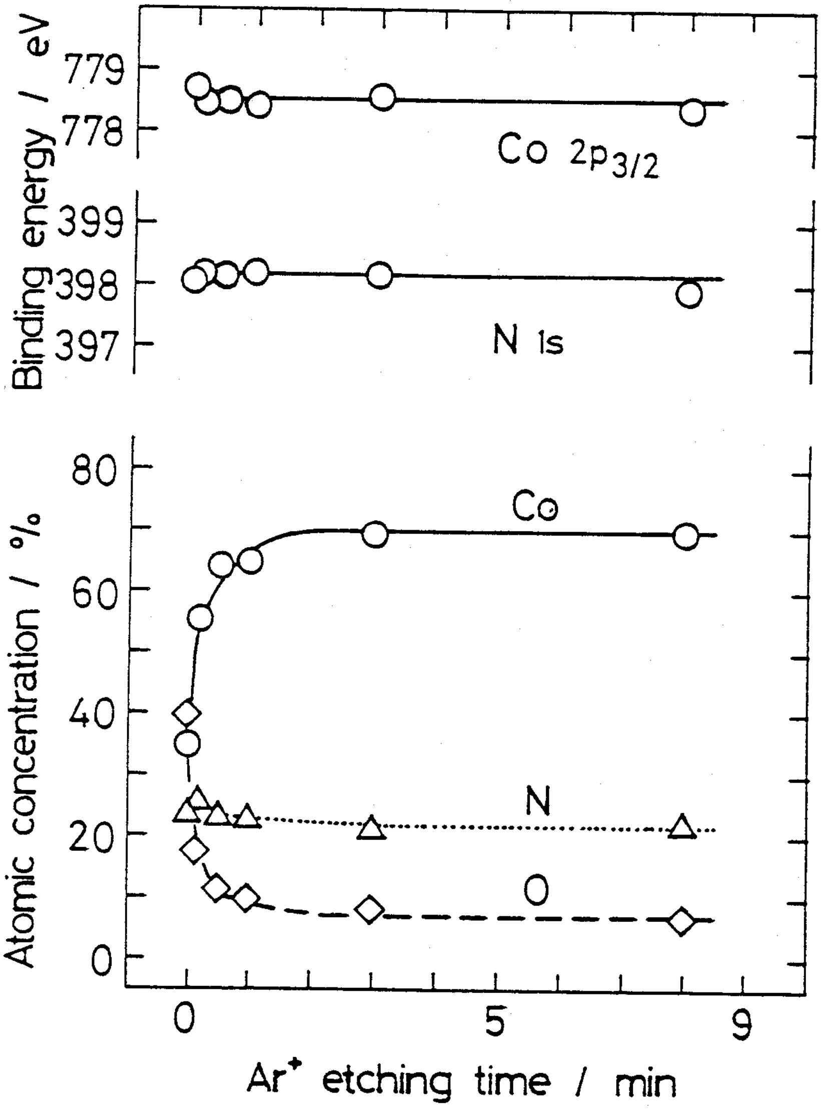

Fig. 3 Relative atomic concentrations for the same Co_xN film as shown in Fig. 2 as a function of the Ar^+-ion etching time, together with the binding energies for the N 1s and the Co $2p_{3/2}$ peaks.

etching time longer than 1 min, suggesting that the deposited film had nearly the same chemical composition as that of crystalline cobalt nitride Co_3N [16]. However, as the above observed atomic ratio is not corrected for the difference in the sputter rate between Co and N, the nitride films in the present work will be designated as Co_xN ($x \gtrsim 3$). It is to be noted that the oxygen concentration in the depth profile of Fig. 3 includes a contribution from contaminating oxygen in the XPS apparatus. The true oxygen concentration in the films can be estimated to be less than 5% from the weak shoulder at about 781 eV in the spectrum (b) of Fig. 2. The binding energy for the Co $2p_{3/2}$ peak for the Co_xN film (778.4 eV) was almost the same as that for cobalt metal, 778.45 eV.

2. Electrochemical Measurements. The Co_xN film electrode is chemically unstable in acidic and alkaline solutions, namely, it dissolves in acidic solutions, and is covered with insulating oxide layers in alkaline solutions. In neutral solutions, e.g., in 0.5 M Na_2SO_4 (pH 6.0), the Co_xN film electrode is stable, though it is electrochemically oxidized and dissolved at potentials more positive than about +0.3 V vs. SCE. Accordingly, the oxygen reduction currents were studied mostly at potentials less positive than ca. 0.1 V.

In Fig. 4, (a) shows a current density(j)-potential(E) curve for a Co_xN film electrode in oxygen-saturated 0.5 M Na_2SO_4 (pH 6.0), (b) that for a smooth Pt electrode, (c) for a Co electrode and (d) for a Co_xN electrode in nitrogen-bubbled 0.5 M Na_2SO_4. In all these electrodes, hydrogen evolution currents start at potentials -1.0 to -1.3 V. Oxygen reduction current in the Co_xN electrode was observed at potentials less positive than +0.1 V. Oxygen reduction current in the Co metal electrode was made obscure by the electrode oxidation (dissolution) current which started at potentials more positive than ca. -0.5 V. The electrode oxidation (dissolution) current for the Co_xN electrode started at ca. +0.3 V, much more positive than the Co metal, as was observed for other metal nitrides (cf. Chapter 2) [14]. However, the j-E curves for the Co_xN electrodes gradually changed during several repeated cyclic scans, especially when the potential was extended to a region more positive than -0.4 V. The

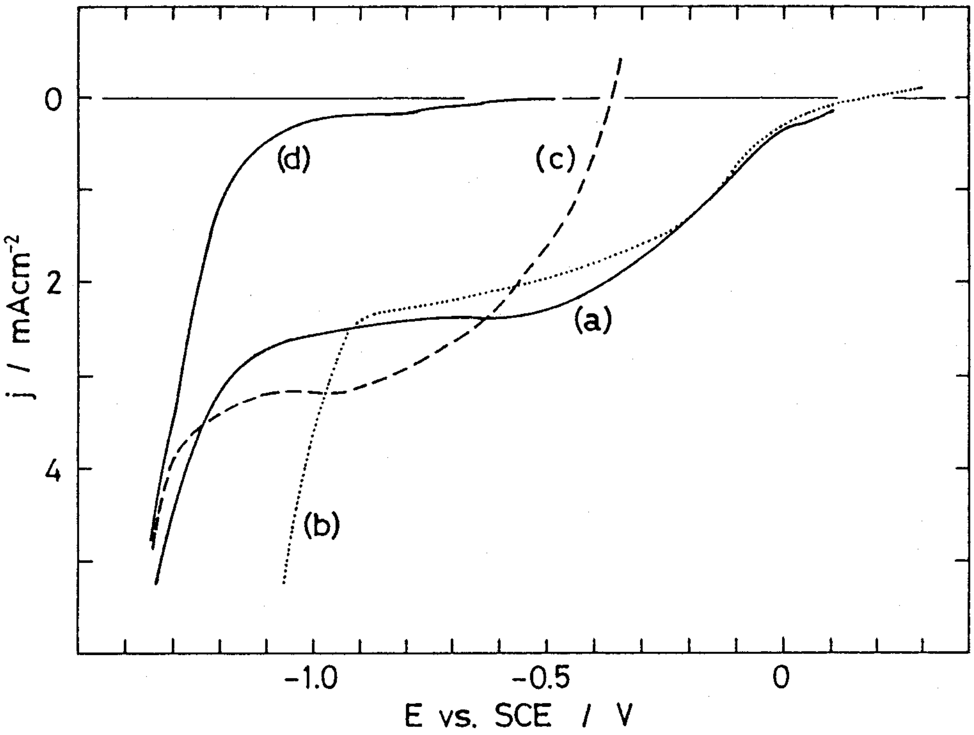

Fig. 4 Current density(j)-potential(E) curves for Co_xN (a), Pt (b) and Co (c) electrodes in O_2-saturated 0.5 M Na_2SO_4 (pH 6.0) and that for Co_xN (d) in deoxygenated 0.5 M Na_2SO_4. The scan rate was 20 mV/s.

j-E curve was restored to the original by chemical etching in 3 M HCl.

Figure 5 shows the disk current(I) vs. E curves measured from negative to positive potentials for the oxygen reduction on a rotating disk (Co_xN) electrode at various rotation frequency (f). They showed a step at around -0.8 V. Figure 6 shows the inverse of I vs. $f^{-1/2}$ (Koutecky-Levich plots [17]) for the Co_xN electrode (a and b) compared with that for a Pt (c) and a glassy carbon (d) electrode. It was reported [18] that the disk current (I) can be expressed as follows:

$$1/I = 1/i_k + 1/i_d \quad (1)$$

$$i_d = Bf^{1/2} \quad (2)$$

$$B = nFAC_rK \quad (3)$$

where i_d and i_k are the diffusion- and the reaction-controlled currents, respectively, n is the number of electrons transfered in the reaction, F the Faraday constant, A the electrode area, C_r the concentration of reactant (O_2), and K is a constant determined by the kinematic viscosity of the solution and the diffusion coefficient for the reactant.

The plots in Fig. 6 show straight lines in all the electrodes. The slope (B^{-1}) for the Co_xN electrode is constant, (7.5 to 8.2) x 10^{-2} mA $(rpm)^{-1/2}$ in a potential region between -0.5 and -0.8 V.

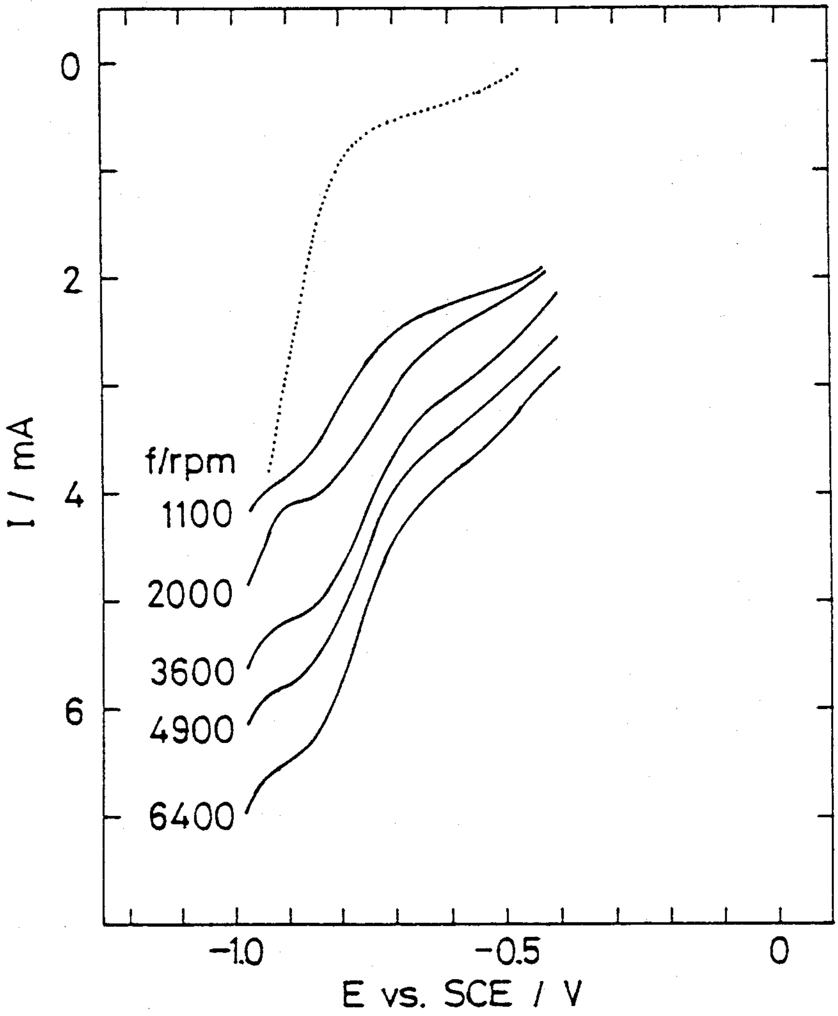

Fig. 5 Current(I)-potential(E) curves for a Co_xN-RDE at various rotation frequencies (f) in O_2-saturated 0.5 M Na_2SO_4 (solid line), as compared with that in deoxygenated 0.5 M Na_2SO_4 (dotted line). The scan rate was 20 mV/s.

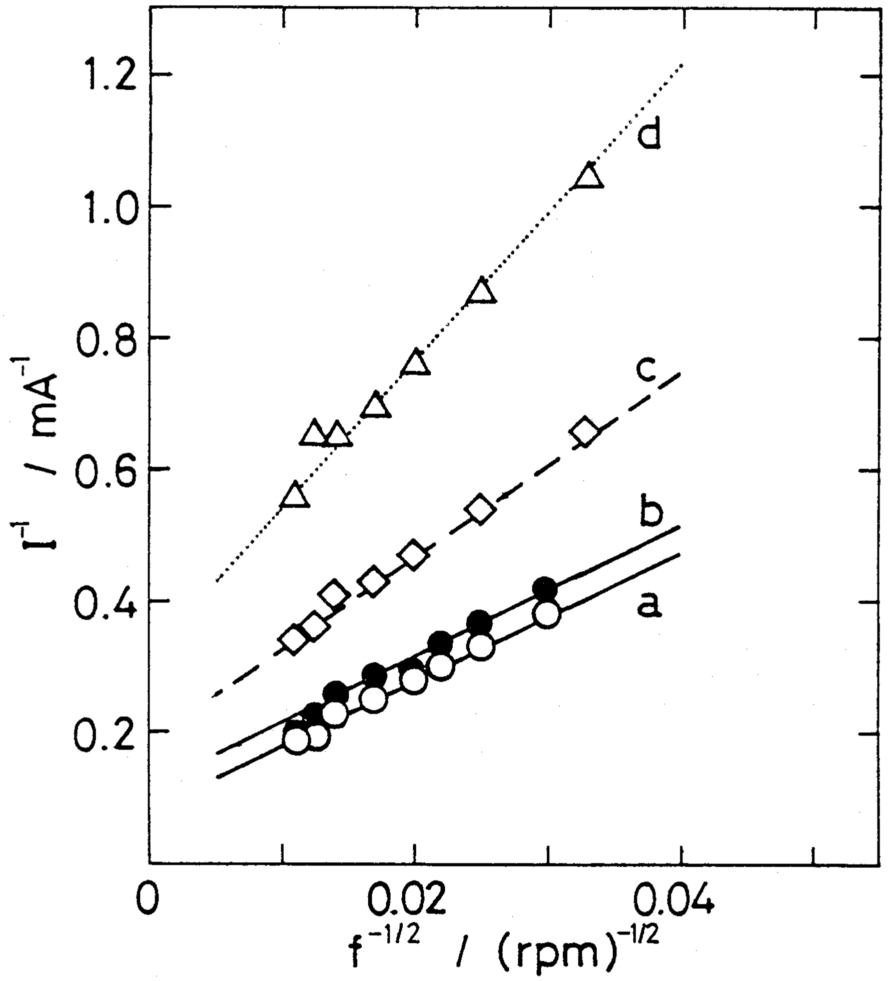

Fig. 6 Kouteckty-Levich plots for the O_2 reduction current (I) at a potential E in oxygenated 0.5 M Na_2SO_4: (a) for Co_xN, E = -0.75 V, (b) for Co_xN, E = -0.70 V, (c) for Pt, E = -0.20 V, and (d) for glassy carbon, E = -0.80 V.

The product of C_r and K in B was determined experimentally to be 2.9×10^{-7} $(rpm)^{1/2}$ mol cm^2 s^{-1} from the observed slope (B^{-1}) of the Koutecky-Levich plot for the glassy carbon (GC) electrode, by assuming that two-electron-transfer type reduction proceeds on the GC electrode, i.e., n = 2 [1]. The electron transfer numbers for the Co_xN and Pt electrodes, calculated by using the above-obtained C_rK value, are given in Table 1, together with the B values. The n value for Pt is 3.30, indicating that both four-electron-transfer type and two-electron-transfer type reductions occur on the Pt electrode, in agreement with the reported results [1]. The n value for the Co_xN electrode was ranged from 3.40 to 3.70, indicating that the four-electron reduction reaction is more dominant than for Pt.

Figure 7 shows a j-E curve for a Co_xN electrode in a deoxygenated 0.5 M Na_2SO_4 solution containing 8.8 mM H_2O_2 (solid line) compared with that in the solution without H_2O_2 (dotted line). It is seen that the reduction of H_2O_2 occurs on the Co_xN electrode in a potential region less positive than about 0.1 V. This result strongly supports the above conclusion that four-electron reduction reaction proceeds on the Co_xN electrode.

Figure 8 shows the results obtained by using a rotating ring (Pt)- disk (Co_xN) electrode (RRDE) in oxygen-saturated 0.5 M Na_2SO_4; the disk current (I_D) and the ring current (I_R) at a constant ring potential E_R = 1.0 V vs. SCE against the disk potential (E_D) are given. The E_R value of 1.0 V was chosen so as

Table 1 The B values for the Koutecky-Levich plots (Fig. 6) and the electron number (n) for the oxygen reduction reaction calculated from them.

Electrode	E (V vs. SCE)	B (x10^{-5} A $(\text{rpm})^{-1/2}$)	n
Pt	-0.15 - -0.40	7.27	3.30
CoN_x	-0.70 - -0.80	7.47 - 8.15	3.40 - 3.70
GC	-0.80 - -0.90	4.39	2.0*

* This value was assumed for the calculation of n for Pt and CoN_x.

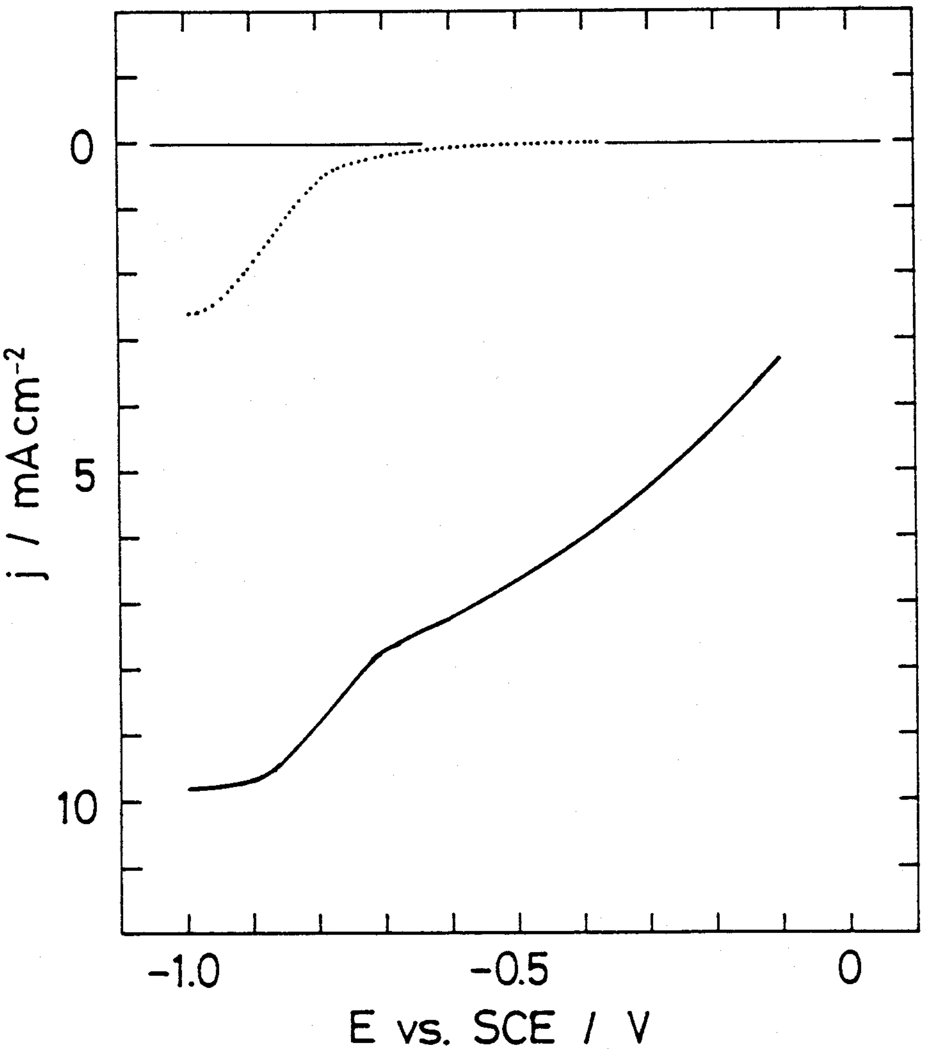

Fig. 7 Current(j)- potential(E) curves for the Co_xN electrode in deoxygenated 0.5 M Na_2SO_4 (solid line) with and (dotted line) without 8.8 mM H_2O_2. The scan rate was 20 mV/s.

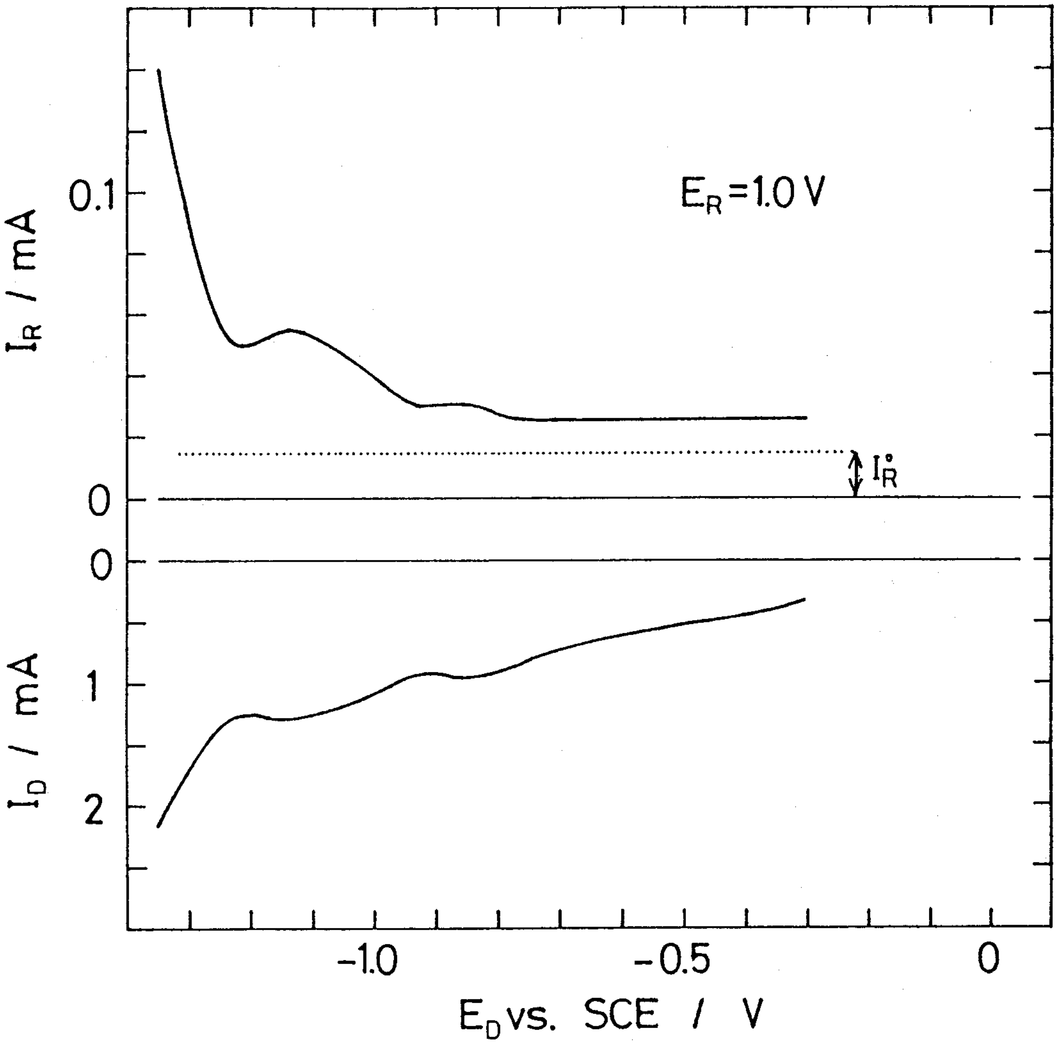

Fig. 8 Disk current (I_D) - disk potential (E_D) and ring current (I_R) - disk potential (E_D) curves for the Co_xN electrode in O_2-saturated 0.5 M Na_2SO_4. The rotation frequency was 3600 rpm, the ring potential E_R was 1.0 V, and the scan rate was 20 mV/s.

to detect H_2O_2 when it was formed by the oxygen reduction on the Co_xN-disk electrode. A small ring current ($I_R^0 \approx 14\ \mu A$) was observed at this E_R even when no disk current flowed. The steeply descending disk current (I_D) in a potential region less positive than -1.2 V is due to the hydrogen evolution on the Co_xN-disk electrode, and the steeply rising ring current (I_R) in the same potential region is due to the re-oxidation of the produced hydrogen on the Pt-ring electrode. The disk current in a potential region between -0.3 and -1.2 V should be due to the oxygen reduction into either H_2O or H_2O_2 on the Co_xN-disk electrode as mentioned before (cf. Fig. 4(a)). Accordingly, the ring current in this potential region, as measured from the above-mentioned I_R^0, should correspond to the re-oxidation of the produced H_2O_2. The current efficiency $\eta(H_2O_2)$ for the H_2O_2 production, i.e., the ratio of the H_2O_2-producing disk current against the total disk current, can be calculated by an equation

$$\eta(H_2O_2) = (I_R - I_R^0) / N \cdot I_D \qquad (4)$$

where N is the current collection efficiency determined by the geometrical structure of the RRDE. In our Co_xN-Pt RRDE, N was determined to be 0.175 by measuring the I_R and I_D in a 10 mM $Fe(CN)_6^{3-}$ solution. The current efficiency $\eta(H_2O_2)$ thus calculated was 4 to 5% at E_D = -0.7 and -0.5 V and 17.4% at -1.1 V.

Discussion

We have found for the first time that the onset potential for the oxygen-reduction current in the Co_xN amorphous film electrodes is rather close to that for Pt electrodes known to be the most active material for the oxygen reduction [8]. Besides, the reaction on this electrode was more prevalently of the four-electron-transfer type than on the Pt electrodes. Unfortunately, the Co_xN film electrodes prepared in the present work were not sufficiently stable near the onset potential of the oxygen reduction current. In spite of this instability, the present result is interesting enough from the view-point that it indicates the influence of nitridation on the reaction mechanism since Co metal electrodes cause only two-electron-transfer type reduction.

It is reported [9] that carbon electrodes modified with $Co-N_4$ chelate compounds such as Co-phthalocyanines and Co-porphyrins have fairly high electrocatalytic activity for the oxygen reduction. However, these compounds cause only two-electron-transfer type reduction into hydrogen peroxide [9] with a head-on type adsorbed oxygen molecule on cobalt as an intermediate [19,20]. On the other hand, two Co-porphyrin held parallel to each other by side alkyl chains (abbreviated as face-to-face Co-Co-4 porphyrins in the literature) are reported to cause four-electron-transfer type reduction [3-7] with the oxygen molecule held in the form of a Co-O-O-Co bridge as a reaction intermediate [4-7]. It is reported also that four-electron-transfer type reduction in such compounds proceeds only when the Co-Co distance is in a range of 0.4 to 0.6 nm [4-6], and that the Co-Co-4 porphyrin forming the cis $_{\mathrm{Co}}\diagup^{\mathrm{O-O}}\diagdown_{\mathrm{Co}}$ bridge configuration show a reaction rate higher than that forming trans configuration [6]. In the Co_xN film electrodes of the present work, the Co atoms are surrounded by several nitrogen atoms, and therefore it can be expected that the electronic structure of the Co atoms is modified by the surrounding N atoms so as to have high electrocatalytic activity similar to the $Co-N_4$ chelates. Also, both the head-on type (Co•••O = O) and the bridge-type (Co•••O = O•••Co) oxygen adsorption are possible stereochemically in the Co_xN electrodes. These facts probably constitute the reason why four-electron-transfer type reduction mainly occurs on the Co_xN electrodes.

As mentioned in the introductory section, the four-electron-transfer type reduction proceeds on metal electrodes such as Pt, Pd and Ag [1]. Gland reported by electron energy loss spectroscopy [21] that oxygen molecules were adsorbed on a single crystal (111) platinum surface in vacuo, taking a side-on (or lateral) structure. On the basis of this result, Clouser reported later [8] that four-electron-transfer type reduction on Pt electrode proceeded via such an adsorbed oxygen, followed by its dissociation. On the other hand, it was discussed [19,20] that two-electron-transfer type reduction in other metal electrodes such as Co was initiated by the head-on type adsorption of oxygen molecules. It should be noted here that the smallest atomic distances in the Pt, Pd and Ag electrodes are nearly the same, i.e., 0.278, 0.276 and 0.288 nm, respectively, and that in the Co metal electrode is somewhat shorter, 0.250 nm. The Co-Co distance in the Co_3N crystal (γ-type, hexagonal) is calculated to be 0.280 nm from the lattice constants a_0 = 0.2658 nm and c_0 = 0.4351 nm [16]. Though the sputter-deposited Co_xN films in the present work are amorphous, they have an x value of about 3 as mentioned before, and we can assume that the Co-Co distance for the amorphous Co_xN ($x \approx 3$) is similar to that for the γ-Co_3N crystal. Thus, the metal-metal distance in the Co_xN film is estimated to be rather close to those for the Pt, Pd and Ag electrodes which cause the four-electron-transfer type reduction, but longer than that of the Co metal electrode which causes the two-electron-transfer type oxygen reduction. Such an increase in the Co-Co distance might play an important role in the oxygen reduction reaction in the Co_xN electrode.

In conclusion, the present study has revealed that the amorphous cobalt nitride (Co_xN) electrode catalyzes the four-electron reduction of oxygen into water like the Pt electrodes, in contrast to the cobalt metal electrodes. This result suggests that the catalytic activity of the Co atoms improved by the coordination of nitrogen atom is in the Co_xN film, as reported for Co-N_4 chelate compounds. It seems significant that the nearest Co-Co distance in the Co_xN film (0.280 nm) is longer than that for the Co metal (0.250 nm) and very close to those for the Pt, Pd and Ag (0.276 to 0.288 nm).

References

1. J. P. Hoare, in A. J. Bard (Ed.) Encyclopedia of Electrochemistry of the Elements, vol. 2, Marcel Dekker, New York, 1974, p. 305.
2. J. Zagal, P. Bindra and E. Yeager, J. Electrochem. Soc., 127 (1980) 1506.
3. J. P. Collman, M. Marrocco, P. Denisevich, C. Koval and F. C. Anson, J. Electroanal. Chem., 101 (1979) 117.
4. J. P. Collman, P. Denisevich, Y. Konai, M. Marrocco, C. Koval and F. C. Anson, J. Am. Chem. Soc., 102 (1980) 6027.
5. R. R. Durand, Jr, C. S. Bencosme, J. P. Collman, J. Am. Chem. Soc., 105 (1983) 2710.
6. H. Y. Liu, M. I. Weaver, C. -B. Wang and C. K. Chang, J. Electroanal. Chem., 145 (1983) 439.
7. C. K. Chang, H. Y. Liu and I. Abdalmuhdi, J. Am. Chem. Soc., 106 (1984) 2725.
8. E. Yeager, Electrochim. Acta, 29 (1984) 1527.
9. A. Van der Putten, A. Elzing, W. Visschen and E. Barendrecht, J. Electroanal. Chem., 205 (1986) 233.
10. N. A. Vante and H. Tributsch, Nature, 323 (1986) 431.
11. M. Azuma, Y. Nakato and H. Tsubomura, Mater. Res. Bull., 22 (1987) 527.
12. M. Azuma, Y. Nakato and H. Tsubomura, J. Electroanal. Chem., 220 (1987) 369.
13. M. Azuma, Y. Nakato and H. Tsubomura, submitted to J.

Electroanal. Chem.

14. M. Azuma, Y. Nakato and H. Tsubomura, submitted to J. Electroanal. Chem.
15. M. Azuma, M. Kashihara, Y. Nakato and H. Tsubomura, submitted to J. Electroanal. Chem.
16. ASTM card, 6-0691.
17. J. Zagal, R. K. Sen and E. Yeager, J. Electroanal. Chem., 83 (1977) 207.
18. J. Newman, J. Phys. Chem., 70 (1966) 1327.
19. B. Z. Nikolic, R. R. Adzic and E. B. Yeager, J. Electroanal. Chem., 103 (1979) 281.
20. B. Simic-Glavaski, S. Zecevic and E. Yeager, J. Phys. Chem., 87 (1983) 4555.
21. J. L. Gland, B. A. Sexton and G. B. Fisher, Surf. Sci., 95 (1980) 587.

Acknowledgment

I wish to express my sincerest gratitude to Professor Hiroshi Tsubomura and Associate Professor Yoshihiro Nakato for their continuing guidance and encouragement during the course of this work. I am grateful to Dr. M. Matsumura, Dr. H. Kobayashi, Professor H. Tamura (Department of Applied Chemistry, Osaka Institute of Technology) and Professor H. Yoneyama (Department of Applied Chemistry, Faculty of Engineering, Osaka University) for their valuable advices and discussions. I would like to thank also the graduate and present students of our laboratory for their collaboration, especially, Mr. M. Kashihara (Chapter 3). Finally, my grateful thanks are also expressed to Professors and Doctors of this Department for their kind advices.

Publication List

1) "Stable and Efficient Electrochemical Evolution of Oxygen and Chlorine on Niobium Nitride Amorphous Thin Films Prepared by the Reactive RF Sputtering Technique"
Masashi Azuma, Yoshihiro Nakato and Hiroshi Tsubomura
Mater. Res. Bull., 22, 527 (1987).

2) "Efficient and Stable Oxygen Evolution on Zirconium Nitride Thin Film Electrodes Prepared by the Reactive RF Sputtering Technique"
Masashi Azuma, Yoshihiro Nakato and Hiroshi Tsubomura
J. Electroanal. Chem., 220, 369 (1987).

3) "Oxygen and Chlorine Evolution on Niobium- and Zirconium-Nitride Amorphous Thin Film Electrodes Prepared by the Reactive RF Sputtering Technique"
Masashi Azuma, Yoshihiro Nakato and Hiroshi Tsubomura
Submitted to J. Electroanal. Chem.

4) "High Electrochemical Stability of Zirconium- and Niobium-Nitride Amorphous Films in Sharp Contrast to Unstable Titanium- and Vanadium-Nitrides"
Masashi Azuma, Yoshihiro Nakato and Hiroshi Tsubomura
Submitted to J. Electroanal. Chem.

5) "Reduction of Oxygen to Water on Cobalt Nitride Thin Film Electrodes Prepared by the Reactive RF Sputtering Technique"
Masashi Azuma, Minoru Kashihara, Yoshihiro Nakato and Hiroshi Tsubomura
Submitted to J. Electroanal. Chem.